Test Plan for Wireless Device Over-the-Air Performance

CTIA 01.90 Informative Reference Material

Version 6.0.2

April 2025

Use Instructions

All testing shall be performed in a CTIA Certification Authorized Test Lab and shall be initiated through one of the following methods:

1. By submitting a PTCRB or IoT Network Certified device certification request at https://certify.ptcrb.com/

2. By submitting an OTA Test Plan use request at https://certify.ctiacertification.org/

CTIA Certification LLC
1400 16th Street, NW
Suite 600
Washington, DC 20036

1.202.785.0081

programs@ctiacertification.org

ctiacertification.org/test-plans/

Table of Contents

List of Figures

List of Tables

Section 1 Introduction

This document is limited to informative content. Certain portions, such as the calculation of spatial averages, may be used normatively by other documents within the test plan by specifying specific requirements.

1.1 Scope

This document provides more details on how various aspects of the test plan were developed and some measurement best practices.

1.2 Acronyms and Definitions

The following specialized terms and acronyms are used throughout this document.

Table 1.2-1 Terms, Acronyms and Definitions

Acronym/Term	Definition
ATL	Authorized Test Lab
CLC	Clenshaw-Curtis
CW	Continuous Wave
DUT	Device Under Test
EIRP	Effective Isotropic Radiated Power
EIS	Effective Isotropic Sensitivity
FDD	Frequency Division Duplexing
LTE	Long Term Evolution
Measurement Points	The individual data points collected during execution of the requisite test methodology.
NHPIS	Near-Horizon Partial Isotropic Sensitivity
NHPRP	Near-Horizon Partial Radiated Power
OTA	Over-The-Air
PIGS	Partial Isotropic GNSS Sensitivity
RB	Resource Block
RS-EPRE	Reference Signal-Energy Per Resource Element
RX	Receive
Test Condition	The emulated propagation conditions utilized within the test system. The test condition is only seen in the validated test volume of the test system.
Test System	The controlled propagation environment used for evaluation of the Device Under Test (DUT).

Acronym/Term	Definition
Test Methodology	The process used to execute tests against the DUT using the Test System(s) and Test Condition(s) specified by this document.
Test Volume	The useable volume within the test system in which the DUT can be placed. The test volume is assumed to have a uniform power distribution within the uncertainty specified by the site validation.
Test Zone	The portion of the test volume in which the test condition criteria are met within the applicable uncertainty limits.
TIS	Total Isotropic Sensitivity
TRP	Total Radiated Power
TX	Transmit
UHIS	Upper Hemisphere Isotropic Sensitivity

1.3 Referenced Documents

Document Number Document Title	
[1]	W.C. Jakes, Editor, Microwave Mobile Communications, John Wiley & Sons, 1974.
[2]	T. Taga, Analysis for Mean Effective Gain of Mobile Antenna in Land Mobile Radio Environments, IEEE Transactions on Vehicular Technology, Vol. 39, No. 2, May, 1990.
[3]	Warren L. Stutzman, Gary A. Thiele, Antenna Theory and Design, 2nd Edition, Wiley& Sons, December 1997.
[4]	Thomson, J. J.(1904), "XXIV. On the structure of the atom: an investigation of the stability and periods of oscillation of a number of corpuscles arranged at equal intervals around the circumference of a circle; with application of the results to the theory of atomic structure," Philosophical Magazine Series 6, 7: 39, 237-265.
[5]	CTIA 01.03, *Normative Reporting Tables*
[6]	CTIA 01.20, *Test Methodology, SISO, Anechoic Chamber*
[7]	CTIA 01.70, *Measurement Uncertainty*
[8]	CTIA 01.73, *Supporting Procedures*
[9]	D. Foster, Loop Antennas with Uniform Current, Proc. IRE, vol. 32, pp. 603-607, October, 1944
[10]	CTIA 01.50, *Wireless Technology, 3GPP Radio Access Technologies*

Section 2 Total Isotropic Sensitivity and Total Radiated Power Derivations (Informative)

This section describes a way of reducing complete spherical patterns of receive-sensitivity or effective isotropic radiated power data to single figures of merit, and to give some meaningful examples of this process. The basic principle applied is to compare the DUT's performance to that of a transceiver with a perfect (100% efficient) antenna.

2.1 Total Isotropic Sensitivity

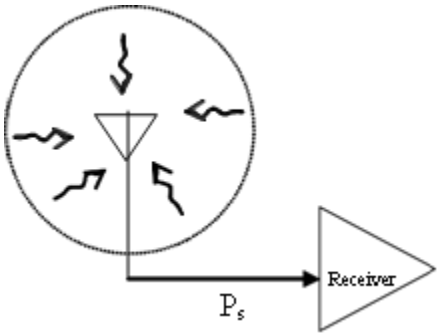

Figure 2.1-1 TIS

This subsection utilizes Yeh's derivation of average received power in the mobile environment as described in Jakes' *Microwave Mobile Communications* [1]. While some equations from that derivation are reproduced here for clarity, the reader is referred to that source for its complete development.

Assume a hypothetical scattered environment which provides equal mean incident powers[1] in both of the orthogonal components E_θ and E_ϕ, and a uniform distribution of angle of incidence (across all θ, ϕ) for both polarizations. Now assume the mean incident powers for both polarizations are simultaneously adjusted (while held equal to one another) so that the average power available to the DUT's receiver from the DUT's antenna when immersed in this environment[1] is equal to the power required for the receiver to operate at its threshold of sensitivity (e.g., a specified bit error rate). If the DUT were now replaced with an ideal isotropic antenna which has equal gain in each linear polarization E_θ and E_ϕ, in every direction, the mean power available from the ideal isotropic antenna immersed in this same scattered environment is defined as the **Total Isotropic Sensitivity**[2], **TIS**, expressed in Watts.

Define the Effective Isotropic Sensitivities, EIS, as follows:

$EIS_\theta(\theta, \phi) =$ Power available from an ideal isotropic, theta-polarized antenna generated by the theta-polarized plane wave incident from direction (θ, ϕ) which, when incident on the DUT, yields the threshold of sensitivity performance.

$EIS_\phi(\theta, \phi) =$ Power available from an ideal isotropic, phi-polarized antenna generated by a phi-polarized plane wave incident from direction (θ, ϕ) which, when incident on the DUT, yields the threshold of sensitivity performance.

---

[1] Most correctly, “immersed in the environment” means the DUT is moved randomly through the (assumed stationary) environment so as to accomplish this averaging of the incident power. In this section, “immersion” is used as shorthand for this hypothetical movement process.

[2] This is a sensible definition because it compares the DUT's antenna/receiver system to a perfect, 100% efficient antenna that responds equally to either polarization.

EIS is the pattern quantity that is actually measured in the chamber during the DUT Measurement Part, by recording power required at each angle and polarization to achieve sensitivity, and is expressed in Watts. It is determined by including the same path-loss factor (as measured at the receive frequency instead of the transmit frequency) that is used in the chamber to yield EIRP for a transmitting antenna. Note that the EIS terms are defined with respect to a single-polarized ideal isotropic antenna, but the TIS is defined with respect to a dual-polarized ideal isotropic antenna. This is a convenience to make the path loss characterization procedure (i.e., the Range Reference Measurement) for receive measurements in the chamber correspond with the path loss characterization procedure done for EIRP. That is to say, the same type of path loss terms, recorded at the appropriate receive frequency, that are generated in the Range Reference Measurement to yield EIRP patterns for a transmit test will yield EIS patterns for a receive test as defined here (based on single-polarized isotropic references). TIS is based on a dual-polarized isotropic comparison, because real-world DUTs and propagation are dual-polarized. Proper choice of integration kernels will be seen to reconcile this apparent difference.

In general, it will be seen in Equation 2.1-1 that:

Equation 2.1-1

$$EIS_x(\theta,\phi) = \frac{P_S}{G_{x,DUT}(\theta,\phi)}$$

where P_S is the radiated sensitivity of the DUT's receiver and $G_{x,DUT}(\theta,\phi)$ is the relative isotropic gain (in polarization x) of the DUT's antenna (in this case, including mismatch and ohmic losses) in the direction (θ,ϕ) . Radiated sensitivity corresponds to the minimum signal power at the radio receiver's input (antenna's output) required to meet the airlink's minimum performance criterion (typically expressed in terms of bit, block or frame error rate). The radiated sensitivity can differ from that found in a conducted test due to interaction factors such as self-desensitization and other non-linear behaviors.

Calculation of Received Power

Following Yeh's derivation of average received power, a right-hand spherical coordinate system (θ,ϕ,r) is utilized, where a_θ and a_ϕ are orthogonal unit vectors associated with θ and ϕ. In the general case, the average power received by an antenna in a scattered environment is (equation 3.1-22 of [1]):

$$P_{rec} = \oint \left[P_1 G_\theta(\Omega) P_\theta(\Omega) + P_2 G_\phi(\Omega) P_\phi(\Omega)\right] d\Omega\,,$$

where Ω is the coordinate point on a spherical surface given by (θ,ϕ), and $d\Omega$ is the differential element of solid angle, $sin(\theta)d\phi d\theta$. This is equivalently written as:

Equation 2.1-2

$$P_{rec} = \oint \left[P_1 G_\theta(\theta,\phi) P_\theta(\theta,\phi) + P_2 G_\phi(\theta,\phi) P_\phi(\theta,\phi)\right] \sin(\theta)\, d\phi d\theta$$

$G_\theta(\theta,\phi)$ and $G_\phi(\theta,\phi)$ are the power gain patterns for the θ and ϕ polarizations, respectively, of the antenna, and $P_\theta(\theta,\phi)$ and $P_\phi(\theta,\phi)$ are the angular density functions of incoming plane waves having θ and ϕ polarizations, respectively, for the environment. P_1 and P_2 are, respectively, the average powers that would be received by a θ- and ϕ- polarized ideal isotropic antenna in the scattered environment.

$P_\phi(\theta,\phi)$ are constants equal to $\frac{1}{4\pi}$ (yielding a uniform distribution of angle of incidence),

and P_1 is equal to P_2. Specifically, P_1 and P_2 are equal to that particular value P_{TIS} which yields the condition of the DUT being at the specified threshold of sensitivity in the hypothetical scattered environment, or $P_1 = P_2 = P_{TIS}$.

For the case of the DUT under these conditions, the mean power delivered by its antenna to its receiver when immersed in this same scattered environment is, by definition, the receiver's sensitivity power, P_S, so that Equation 2.1-2 becomes:

Equation 2.1-3

$$P_S = \frac{P_{TIS}}{4\pi} \oiint \left[G_{\theta,DUT}(\theta,\phi) + G_{\phi,DUT}(\theta,\phi) \right] \sin(\theta)\, d\phi d\theta$$

for the DUT which has antenna gain patterns $G_{x,DUT}(\theta,\phi)$ and is immersed in the scattered environment.

The ideal isotropic dual-polarized antenna envisioned in the definition of TIS would have a total power gain in every direction of 1 (that is, 0 dBi). Therefore, its component gains in each polarization in every direction are 1/2 (that is, -3 dBi), $G_\theta(\theta,\phi) = G_\phi(\theta,\phi) = 1/2$. Hence, substituting into, the average received power for the dual-polarized isotropic antenna in the described environment, TIS, is seen to be:

Equation 2.1-4

$$TIS = \oint \left[P_{TIS} \cdot \frac{1}{2} \cdot \frac{1}{4\pi} + P_{TIS} \cdot \frac{1}{2} \cdot \frac{1}{4\pi} \right] \sin(\theta)\, d\phi d\theta = \frac{P_{TIS}}{4\pi} \oint \sin(\theta)\, d\phi d\theta = P_{TIS}$$

Turning to the EIS definitions, for example that of $EIS_\theta(\theta,\phi)$, Equation 2.1-1 can also be justified. The $EIS_\theta(\theta,\phi)$ measurement refers to an average received power with a single θ-polarized plane wave incident on the DUT from a particular direction (θ,ϕ). As shown by Taga [2], this particular case can also be treated using Equation 2.1-2 by setting:

$$P_\theta(\theta,\phi) = \frac{\delta(\theta-\theta_S)\delta(\phi-\phi_S)}{\sin(\theta)}$$

and

$$P_\phi(\theta,\phi) = 0$$

Where $\delta(x)$ is the dirac delta function and (θ_S,ϕ_S) represents a particular direction for which the EIS is being evaluated. Substituting into for the EIS case (and recalling that the received power in this case is defined to be the sensitivity power, P_S), we have:

$$P_S = \oint \left[P_{1,EIS} G_{\theta,DUT}(\theta,\phi) \frac{[\delta(\theta-\theta_S)\delta(\phi-\phi_S)]}{\sin(\theta)} + 0 \right] \sin(\theta)\, d\phi d\theta = P_{1,EIS} G_{\theta,DUT}(\theta_S,\phi_S)$$

where $P_{1,EIS}$ is just the mean incident power constant that yields the threshold of sensitivity for the DUT at the angle (θ_S,ϕ_S) .

For the θ -polarized ideal isotropic antenna envisioned in the definition of $EIS_\theta(\theta,\phi)$, its gain function is

$G_\theta(\theta,\phi) = 1$ (that is, 0 dBi) and $G_\phi(\theta,\phi) = 0$. Similarly substituting these into Equation 2.1-2 yields:

$$EIS_\theta(\theta_S,\phi_S) = \oint \left[P_{1,EIS} \cdot 1 \cdot \frac{[\delta(\theta-\theta_S)\delta(\phi-\phi_S)]}{\sin(\theta)} + 0\right] \sin(\theta)\, d\phi d\theta = P_{1,EIS}$$

Combining these last two equations, we have:

$P_S = EIS_\theta(\theta_S,\phi_S) G_{\theta,DUT}(\theta_S,\phi_S)$,

for the particular evaluation point (θ_S,ϕ_S), or more generally for the function at any angle,

$$P_S = EIS_\theta(\theta,\phi) G_{\theta,DUT}(\theta,\phi)$$

A similar development would yield the analogous expression for $EIS_\phi(\theta,\phi)$, and these two results lead directly to Equation 2.1-1.

Hence, we can rearrange Equation 2.1-1 so that:

$$G_{x,DUT}(\theta,\phi) = \frac{P_S}{EIS_x(\theta,\phi)}$$

Substituting into Equation 2.1-3 yields:

$$P_S = \frac{P_{TIS}}{4\pi} \oint \left[\frac{P_S}{EIS_\theta(\theta,\phi)} + \frac{P_S}{EIS_\phi(\theta,\phi)}\right] \sin(\theta)\, d\phi d\theta$$

This can be rearranged to yield:

$$P_{TIS} = \frac{4\pi}{\oint \left[\frac{1}{EIS_\theta(\theta,\phi)} + \frac{1}{EIS_\phi(\theta,\phi)}\right] \sin(\theta)\, d\phi d\theta}$$

Substituting this into Equation 2.1-4 yields:

Equation 2.1-5

$$TIS = \frac{4\pi}{\oint \left[\frac{1}{EIS_\theta(\theta,\phi)} + \frac{1}{EIS_\phi(\theta,\phi)}\right] \sin(\theta)\, d\phi d\theta}$$

Results for a few Special Cases

Assume that the receiver, environment, and antenna are all at the same temperature, e.g., 290K.

Case 1: The DUT employs a 100% efficient, single-polarized, ideal isotropic radiator: For example, assume the DUT's antenna is an ideal, theta-polarized isotropic antenna. By definition, $EIS_\theta(\theta,\phi)$ is then P_S for every angle, and $EIS_\phi(\theta,\phi)$is infinite at every angle.

Then Equation 2.1-5 becomes:

$$TIS = \frac{4\pi}{\oint\left[\frac{1}{P_S}+\frac{1}{\infty}\right]\sin(\theta)\,d\phi d\theta} = \frac{4\pi}{\oint\left[\frac{1}{P_S}+0\right]\sin(\theta)\,d\phi d\theta} = \frac{P_S 4\pi}{\oint\sin(\theta)\,d\phi d\theta} = P_S$$

In other words, TIS of an DUT with a 100% efficient, ideal isotropic, single-polarized antenna is just the sensitivity power, P_S.

Case 2: The DUT employs a 100% efficient, dual-polarized, ideal isotropic radiator $EIS_\theta(\theta,\phi)$: is then $2P_S$ for every angle, and $EIS_\phi(\theta,\phi)$ is also $2P_S$ at every angle. (Recall that the EIS is defined with respect to a single-polarized isotropic, and a dual-polarized isotropic antenna must have half the gain in each polarization of a corresponding single-polarized isotropic antenna.) Then Equation 2.1-5 becomes:

$$TIS = \frac{4\pi}{\oint\left[\frac{1}{2P_S}+\frac{1}{2P_S}\right]\sin(\theta)\,d\phi d\theta} = \frac{P_S 4\pi}{\oint\sin(\theta)\,d\phi d\theta} = P_S$$

Again, an DUT with a 100% efficient, ideal isotropic antenna has a TIS that is equal to the conducted sensitivity of the receiver, P_S.

Case 3: The DUT employs a 50% efficient but otherwise ideal, single-polarized isotropic antenna. $EIS_\theta(\theta,\phi)$ is then $2P_S$ for every angle (the antenna is a 3 dB attenuator, degrading the receiver noise figure by 3 dB, so twice the power is required to get the same performance), and $EIS_\phi(\theta,\phi)$ is infinite at every angle. Thus, Equation 2.1-5 becomes:

$$TIS = \frac{4\pi}{\oint\left[\frac{1}{2P_S}+\frac{1}{\infty}\right]\sin(\theta)\,d\phi d\theta} = \frac{4\pi}{\oint\left[\frac{1}{2P_S}+0\right]\sin(\theta)\,d\phi d\theta} = \frac{2P_S 4\pi}{\oint\sin(\theta)\,d\phi d\theta} = 2P_S$$

Therefore, an DUT with a 50% efficient antenna has a TIS equal to the conducted sensitivity degraded by 3 dB (i.e., twice as large).

This supports two general conclusions. First, the lower limit (best achievable value) for TIS is simply the conducted sensitivity of the DUT's receiver, P_S. This TIS is achieved with a perfectly matched, 100% efficient antenna. Second, the TIS of a real antenna will be the conducted sensitivity of its receiver degraded by the mismatch/efficiency loss of the antenna.

2.1.1 Total Isotropic Sensitivity Estimator Based on RSS-Based Methods

For the purposes of TIS, the “threshold of sensitivity performance” would be that point at which the wireless device just passes the sensitivity test; that is, EIS for a given angle/polarization is the minimum RF power level where the radiated sensitivity test still passes.

Because each EIS measurement can be very time-consuming, a complete spherical TIS measurement performed by repeating the sensitivity test to determine every EIS point on the sphere would require extensive test time. Hence the ability to accurately estimate the EIS pattern, and thus the resultant TIS, in a reduced timeframe is critical to minimize the overall test time required to certify a product. The basic approach is to make a minimum number (generally only one) of direct EIS measurements, and then to substitute other less-time-consuming means of capturing the pattern shape information needed to

determine the entire EIS pattern. Since this process relies on the repeatability of a single-point EIS measurement, rather than the integrated result of many single-point EIS measurements, some increase in uncertainty will be incurred.

The basic approach is to directly measure EIS at a single angle/polarization, and then to provide the pattern information through the use of receive signal strength (RSS) measurements reported by the DUT (for some technologies like GPS this may be C/N_0 or some other indicator of the received signal strength), which is a quick measurement that can be performed at all the other angles of the sphere.

To accomplish this in a radiated test chamber, incident field on the DUT is raised by some practical amount (typically 20 dB or so) above the point where the DUT is operating at its threshold of sensitivity on its pattern peak, and then fixed there for the remainder of the pattern measurement process. Ideally this level is near the top of the linear portion of whatever RSS report the DUT can produce, but must not be above the maximum RSS value the DUT can report. At each angle/polarization, the RSS reported by the DUT is recorded as the pattern value for that angle/polarization.

In addition to the RSS pattern information, an RSS linearization curve is required to “calibrate” the data reported by the DUT. This creates a transfer standard between the DUT and the calibrated signal generator (base station simulator, satellite simulator, etc.) used to generate the downlink signal. Because the TIS is primarily determined by peaks in the RSS pattern, which tend to cover more surface area than nulls, the linearization is critical within at least the first 10 dB below the pattern peak. While ideally the linearization should be evaluated across the entire range of RSS values recorded in the pattern, for pattern nulls more than 10 dB below the peak, extrapolation may be used to determine the remaining linearization correction. Normally, the linearization should be determined in an over-the-air configuration for one polarization at the peak of the pattern, but conducted linearization curves may be used in certain circumstances provided additional uncertainty terms are applied to the result.

The linearization curve can be treated as a function of the output power of the signal generator such that the measured RSS is given by:

$$RSS_i = \mathrm{RSS}\left(P_{SG_i}\right)$$

Assuming that the RSS data is monotonic, an inverse function can be defined such that:

$$RSS_i = \mathrm{RSS}\left(\mathrm{RSS}^*(RSS_i)\right)$$

so that:

$$P_{SG_i} = \mathrm{RSS}^*(RSS_i)$$

The conversion from RSS to power may use linear interpolation or curve fitting as necessary to fill in between measured and reported RSS and power steps. The assumption for currently defined RSS based metrics is that linear interpolation is done in dB, not linear power units, although this could be different for other technologies. Note that in cases where interpolation between points may not be the best solution, best fit lines or curves could produce an RSS^* relationship that does not lie directly on the measured linearization data.

Once all of the measured RSS values in the pattern have been linearized, the pattern should be normalized by dividing each pattern value by the peak value in linear power units (equivalent to subtracting the peak from the pattern in dB). The entire process can be represented by the following equation:

$$P(\theta, \phi, Polarization) = \mathrm{RSS}^*\left(RSS(\theta, \phi, Polarization)\right)/\mathrm{RSS}^*(RSS_{Peak}) \ ,$$

where $RSS_{Peak}$is the maximum RSS determined in the pattern (for GNSS this may be the maximum RSS determined in the upper hemisphere of the pattern). The result is a relative pattern with a peak value of 1.0 (0 dB) for any polarization.

A full EIS measurement is performed at the same peak position and polarization to determine a reference for the resultant estimated EIS pattern, which is then given by:

$$EIS(\theta, \phi, Polarization) = EIS_{ref}/P(\theta, \phi, Polarization)$$

where all terms are in linear power units. Alternately the EIS pattern can be determined by subtracting the relative pattern from the reference EIS value in dB. From this point, the previously defined integrals can be used to determine TIS and the various partial surface integrals required for a given technology.

This linearization and normalization method can be repeated to reduce the resultant measurement uncertainty by normalizing to multiple EIS reference values around the surface of the sphere and then averaging the resulting patterns. Through this process, the uncertainty associated with using a single EIS reference can be reduced by a factor of $\frac{1}{\sqrt{N}}$ where N is the number of EIS points used to determine the average EIS pattern.

2.2 Total Radiated Power

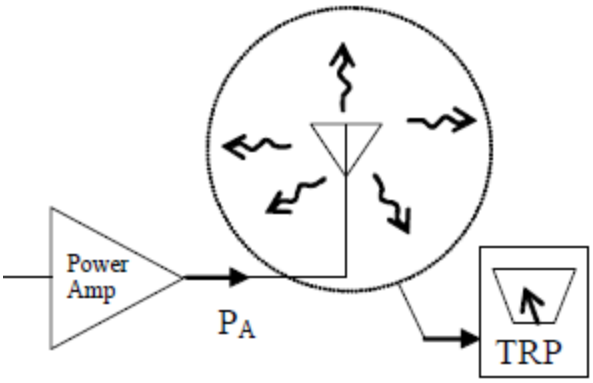

Figure 2.2-1 TRP

Definitions

P_A = Power delivered to the antenna (properly, the power available to the actual antenna load), in W

TRP = Total Radiated Power, the power that is actually radiated by the antenna, in W

The TRP is the sum of all power radiated by the antenna, regardless of direction or polarization. If the antenna were enclosed in a perfectly absorbing sphere, the TRP would be the power that would be absorbed by that sphere. TRP can be related to P_A in this fashion:

Equation 2.2-1

$$TRP = P_A \cdot eff$$

Where

eff = Radiation efficiency of the antenna

The radiation efficiency, eff, is defined in most antenna textbooks as the ratio of the power radiated by an antenna to the power delivered to the antenna. The power delivered to the antenna may differ from the output of the power amplifier into a 50 ohm load due not only to antenna mismatch, but also any non-linear interaction factors induced in the active circuitry.

Derivation of Total Radiated Power

The Total Radiated Power of a given antenna and source is (see, for example, *Stutzman & Thiele* [3], page 33, equation 1-131):

$$TRP = \oint U(\theta,\phi) d\,\Omega\,,$$

Where $U(\theta,\phi)$ = radiation intensity at each angle in Watts/steradian.

Expanding this integral

$$TRP = \int_{\theta=0}^{\pi}\int_{\phi=0}^{2\pi} U(\theta,\phi)\sin(\theta)\,d\phi d\theta$$

It is seen that the $\sin(\theta)$ term results simply from the mathematical expansion of the differential element of solid angle, $d\Omega$:

$$d\Omega = \sin(\theta)\,d\phi d\theta\,,$$

The effective isotropic radiated power, EIRP, is defined as (Stutzman & Thiele [3], page 62, equations 1-226 and 1-227):

$$EIRP(\theta,\phi) = P_T G_T(\theta,\phi) = 4\pi U(\theta,\phi)\,,$$

Where $P_T G_T$ is the product of the power delivered to the antenna and the antenna's power gain. (The equation cited in the reference is actually for the specific case of peak EIRP at the angle of maximum gain, but the reasoning used in the reference produces the above equation for the more general EIRP vs. angle function.)

Then we have:

$$U(\theta,\phi) = \frac{EIRP(\theta,\phi)}{4\pi},$$

And the integral for TRP becomes

Equation 2.2-2

$$TRP = \frac{1}{4\pi}\int_{\theta=0}^{\pi}\int_{\phi=0}^{2\pi} EIRP(\theta,\phi)\sin(\theta)\,d\phi d\theta$$

Thus, if the complete spherical pattern of the EIRP of the DUT is integrated with the $\sin(\theta)$ weighing as described in this equation, the result will be the total power the DUT is radiating. It should be noted here that this integration would be modified to yield the same total radiated power if the pattern measurement is expressed in terms of ERP (effective radiated power referenced to a half-wave dipole) rather than EIRP. Specifically, ERP is numerically 2.14 dB less than EIRP:

$$ERP(\theta,\phi) \cong \frac{EIRP(\theta,\phi)}{1.64},$$

So that:

$$TRP \cong \frac{1.64}{4\pi}\int_{\theta=0}^{\pi}\int_{\phi=0}^{2\pi} ERP(\theta,\phi)\sin(\theta)\,d\phi d\theta$$

It must be emphasized that, whether the pattern data itself is taken in the form of ERP or EIRP, use of the appropriate integration will yield numerically the same TRP (as well it should-the DUT is radiating the same power in either case).

In practice, the total EIRP will likely be measured at each sample point by measuring its two orthogonally polarized components, $EIRP_{\theta}(\theta,\phi)$ and $EIRP_{\phi}(\theta,\phi)$.To accommodate this measurement practicality, we can split the radiation intensity at each angle into two contributions, one from each polarization (power in independent components simply adds):

$U_{\theta}(\theta,\phi)$ = Radiation intensity due to theta component of E-field

$U_{\phi}(\theta,\phi)$ = Radiation intensity due to phi component of E-field Then Equation 2.2-2 can be re-derived as:

$$TRP = \frac{1}{4\pi}\int_{\theta=0}^{\pi}\int_{\phi=0}^{2\pi}\left[EIRP_{\theta}(\theta,\phi) + EIRP_{\phi}(\theta,\phi)\right]\sin(\theta)\,d\phi d\theta$$

Section 3 Calculating Spatially Averaged Quantities and Numerical Integrals of Discretely Sampled Pattern Data

For traditional omni-directional antennas, the required figures of merit are based on the spatially averaged EIRP and EIS. When averaged over the full spherical surface about the DUT (i.e. at the infinitesimal limit), these metrics are mathematically equivalent to the total power quantities of TRP and TIS. In addition, the EIRP and EIS can be averaged over a subset of the surface to obtain various partial surface quantities.

For the steerable antenna patterns such as those for 5G NR FR2, the choice was made to use a cumulative distribution function (CDF) of the peak EIRP and minimum EIS of each beam in order to determine spherical coverage of the DUT, rather than reporting the spatial average of the peak EIRP. The total radiated power of the peak beam is also determined, but does not represent the spatially averaged performance of the DUT like that for omni-directional antennas.

3.1 Grid Types

Several different measurement grid types are allowed, depending on the test requirement.

3.1.1 Constant Angular Step Size

The constant angular step size grid type has the measured data points uniformly distributed as a function of theta and phi angles as illustrated in 2D in Figure 3.1.1-1 and in 3D in Figure 3.1.1-2.

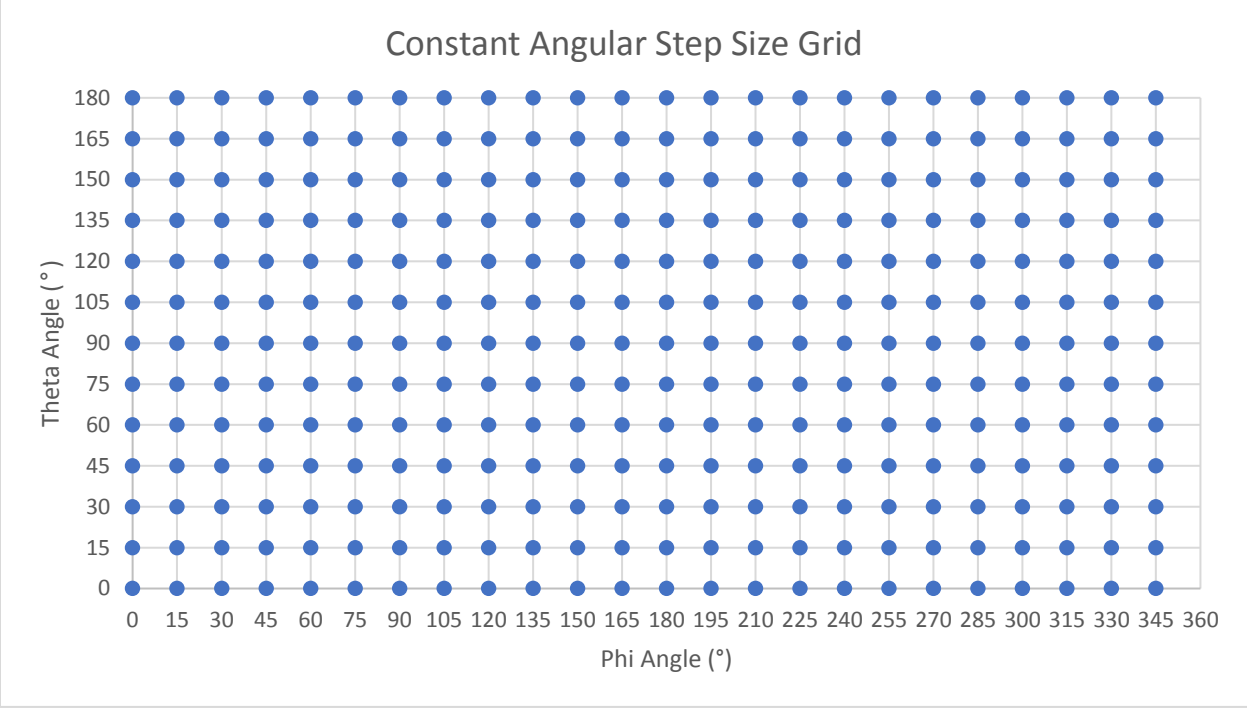

Figure 3.1.1-1 Sample Distribution of Measurement Grid Points in 2D for a Constant Step Size Grid with $\Delta\theta = \Delta\phi = 15°$ (Note that redundant points are plotted at the poles for $\theta = 0°$ and $180°$ for 312 points, while there are only 266 unique measurement points)

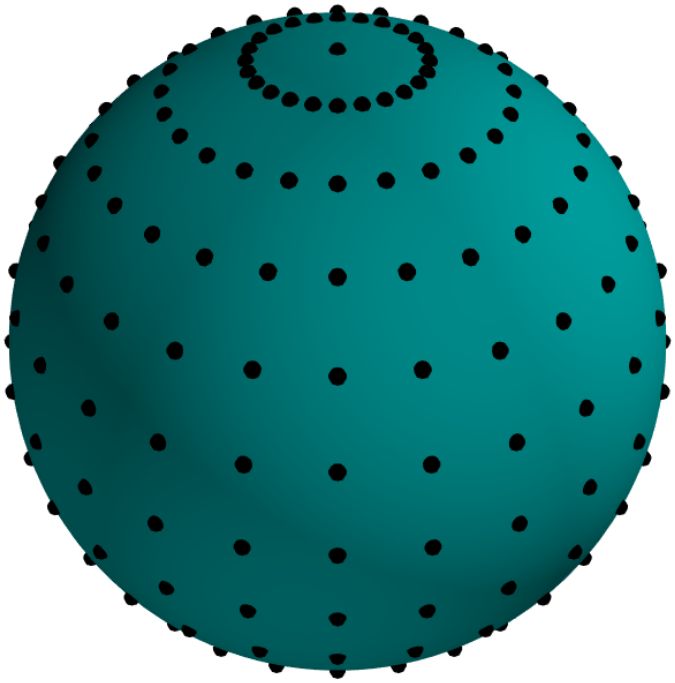

Figure 3.1.1-2 Sample Distribution of Measurement Grid Points in 3D for a Constant Step Size Grid with $\Delta\theta = \Delta\phi = 15°$ (266 unique measurement points)

3.1.2 Theta Dependent Phi Optimization

Since evenly spaced points in phi become closer together on the spherical surface as theta approaches the poles at 0 and 180 degrees, essentially oversampling the surface near the poles, the theta dependent phi optimization allows reducing the number of measured data points as a function of theta. While the choice of starting point for each phi cut has an impact on the surface spacing of the measured points, an appropriate choice can produce a quite uniform surface spacing as illustrated in 2D in Figure 3.1.2-1 and in 3D in Figure 3.1.2-2.

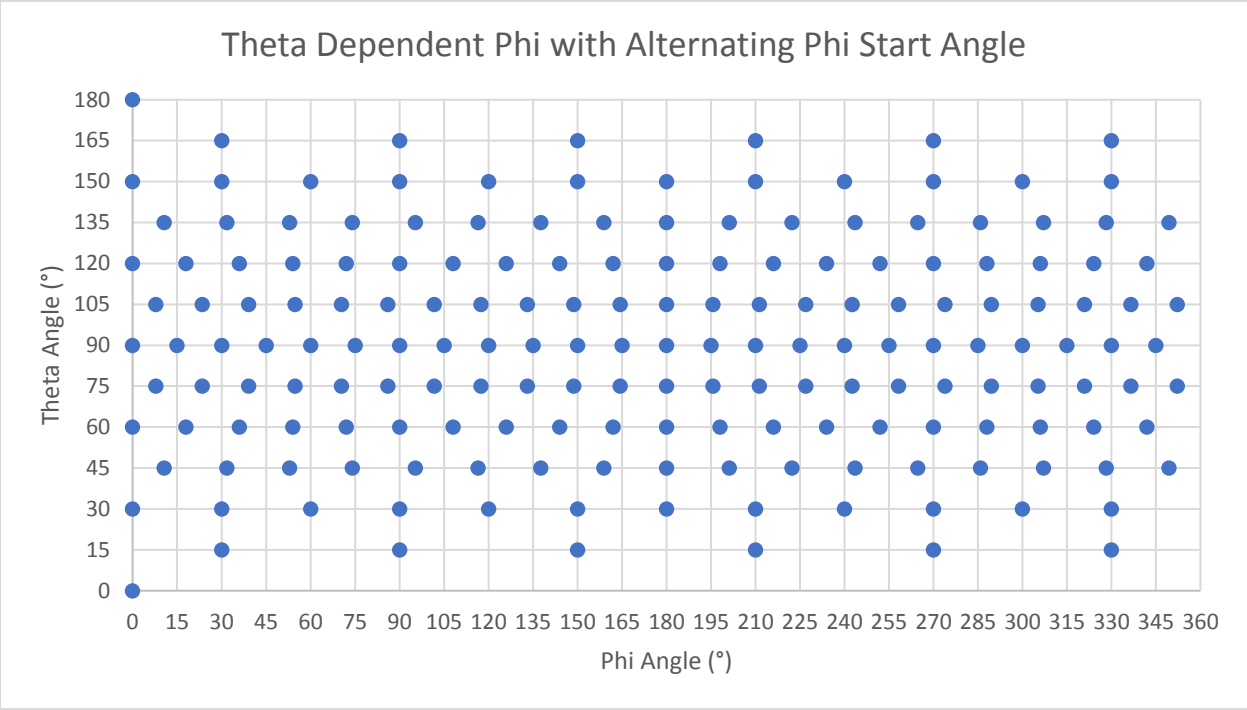

Figure 3.1.2-1 Sample Distribution of Measurement Grid Points in 2D for a Theta Dependent Phi Step Size Grid with Δθ=15° (182 unique measurement points)

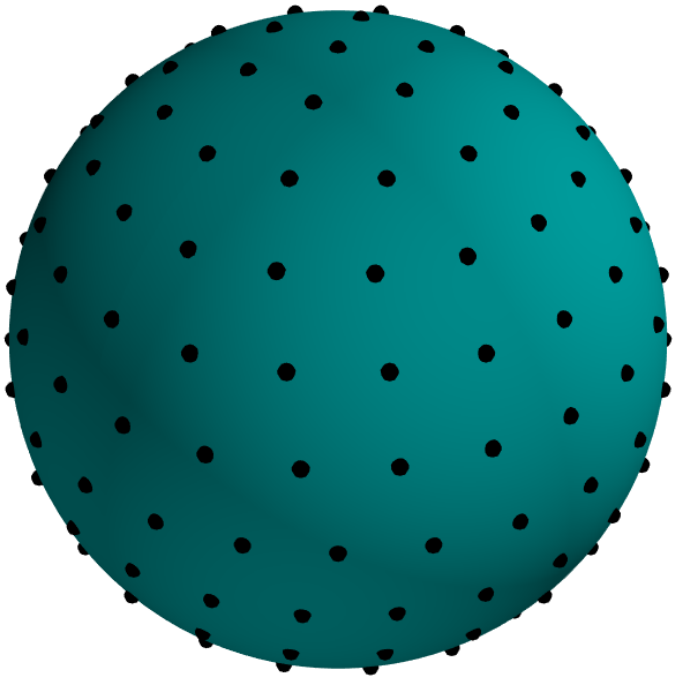

Figure 3.1.2-2 Sample Distribution of measurement grid points in 3D for a theta dependent phi step size grid with $\Delta\theta = 15°$ (182 unique measurement points)

3.1.3 Constant Density

Theta dependent phi is a first approximation to a constant density grid which has measurement points that are evenly distributed on the surface of the sphere with an equal spacing. After evaluating various methods, the charged particle approach (see *On the Structure of the Atom* [4]), where the resulting grid points produce a minimum energy configuration of equally charged particles confined to the surface of a unit sphere, was chosen as the best implementation of the constant density grid with nearly equal spacing between grid points. A suitable Matlab implementation can be found at https://www.mathworks.com/matlabcentral/fileexchange/37004-suite-of-functions-to-perform-uniform-sampling-of-a-sphere. Since the resulting grid is dependent on the chosen number of charged particles (measurement points), the random number seed used for initial placement of those points, and the number of iterations used for convergence, each generated set of grid points may be unique and thus no standard set of grid points has been defined. One example of this grid spacing is illustrated in 2D in Figure 3.1.3-1 and in 3D in Figure 3.1.3-2.

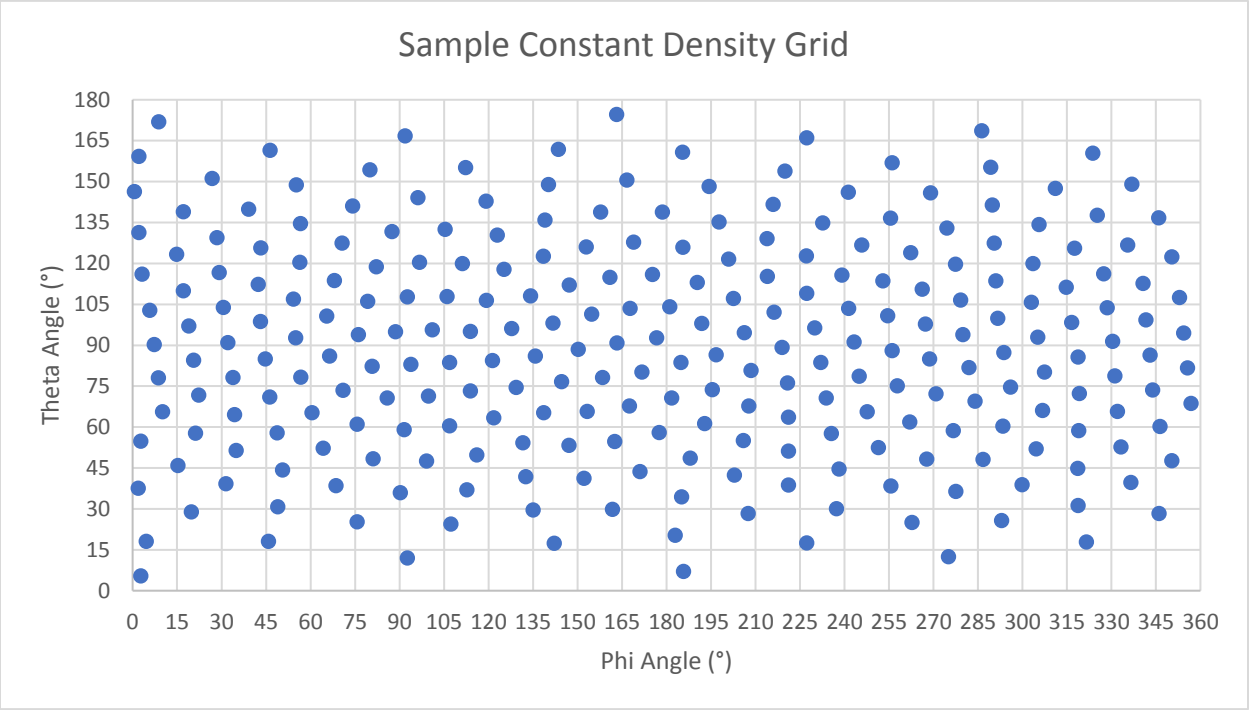

Figure 3.1.3-1 Sample Distribution of Measurement Grid Points in 2D for a Constant Density Grid with 266 Unique Measurement Points

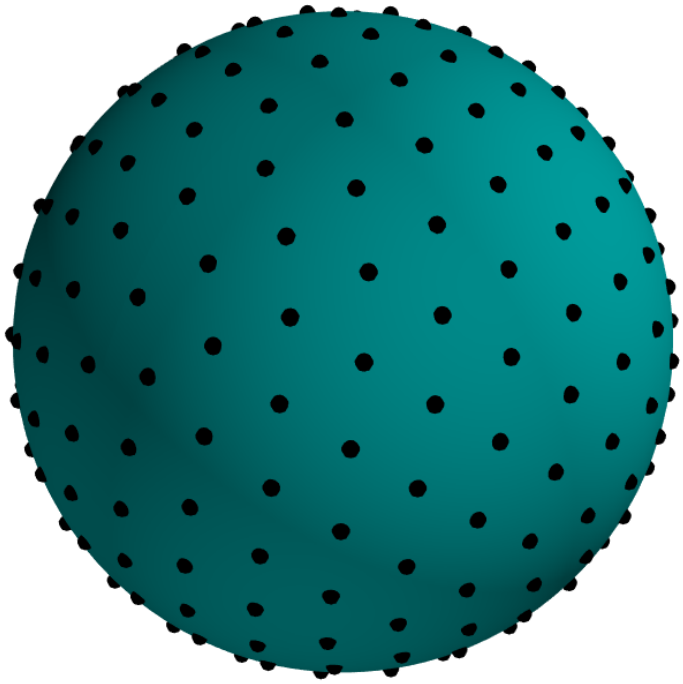

Figure 3.1.3-2 Sample Distribution of Measurement Grid Points in 3D for a Constant Density Grid Type with 266 Unique Measurement Points

3.1.4 Spiral Scans

Where measurement samples can be taken rapidly (e.g. transmit power measurements), an alternate to the fixed step size grid, where measurements are performed at specific positions, is to acquire data on the fly as positioners are moving. This results in a spiral grid arrangement since both theta and phi are changing simultaneously. Note that while the most common approach is to spiral from pole to pole with theta moving from 0-180 degrees while phi makes multiple revolutions, systems capable of great circle acquisition could also generate polar spirals where the theta axis makes multiple revolutions as phi moves from 0 to 180 degrees.

Figure 3.1.4-1 illustrates the grid spacing for a constant velocity conical spiral meeting the minimum 15-degree resolution, while Figure 3.1.4-2 shows this same data in 3D.

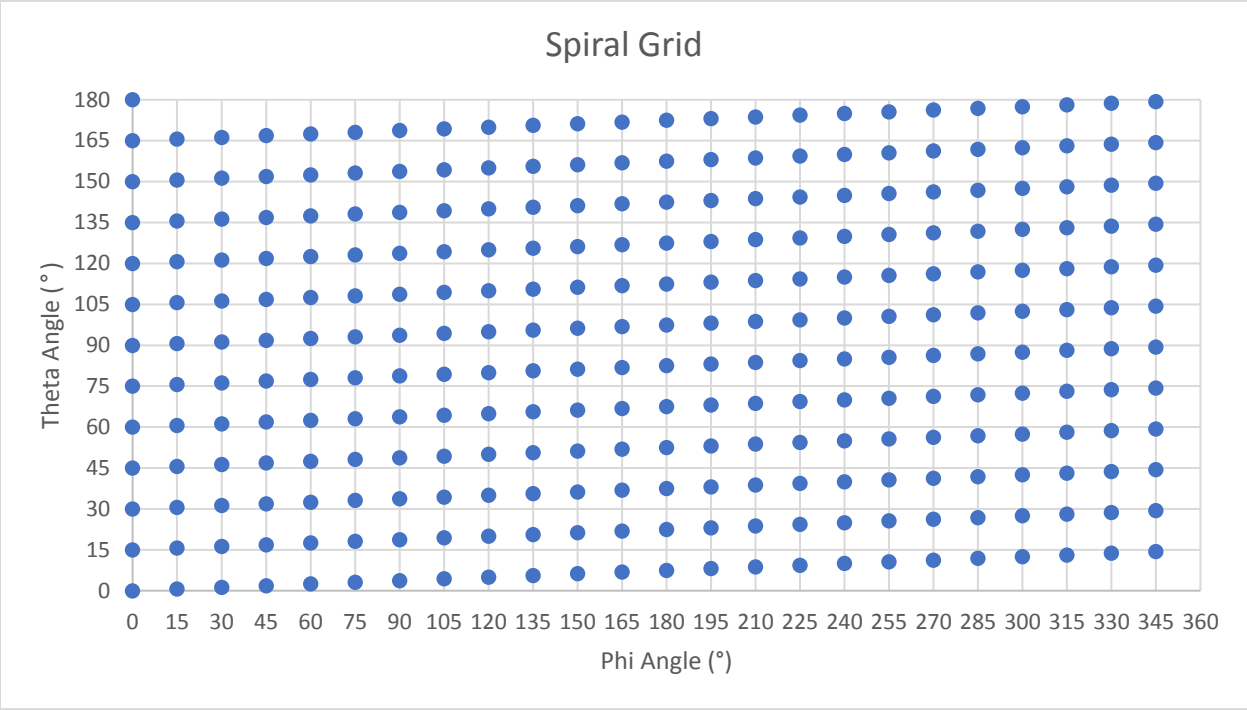

Figure 3.1.4-1 Sample Distribution of Measurement Grid Points in 2D for a Constant Velocity Spiral Scan Grid with 289 Unique Measurement Points

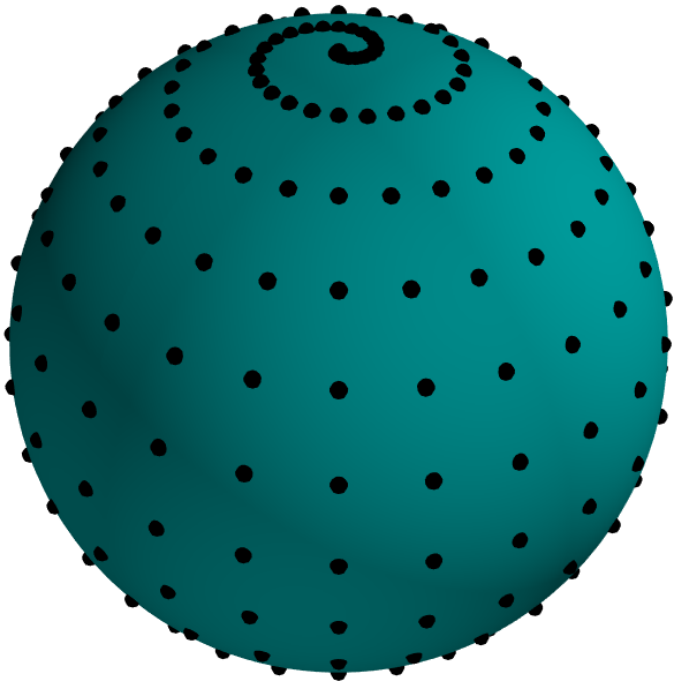

Figure 3.1.4-2 Sample Distribution of Measurement Grid Points in 3D for a Constant Velocity Spiral Scan Grid with 289 Unique Measurement Points

The polar spiral grid looks very similar, but with the theta and phi axes flipped. However, on the spherical surface, the resulting grid is much closer to the constant angular grid spacing, although the “seam” between the front and back hemispheres of the grid are tilted in opposite directions. For this reason, it is best to still start the sweep at one pole (e.g. $\theta = 0°$) and end at the other (e.g. $\theta = 180°$).

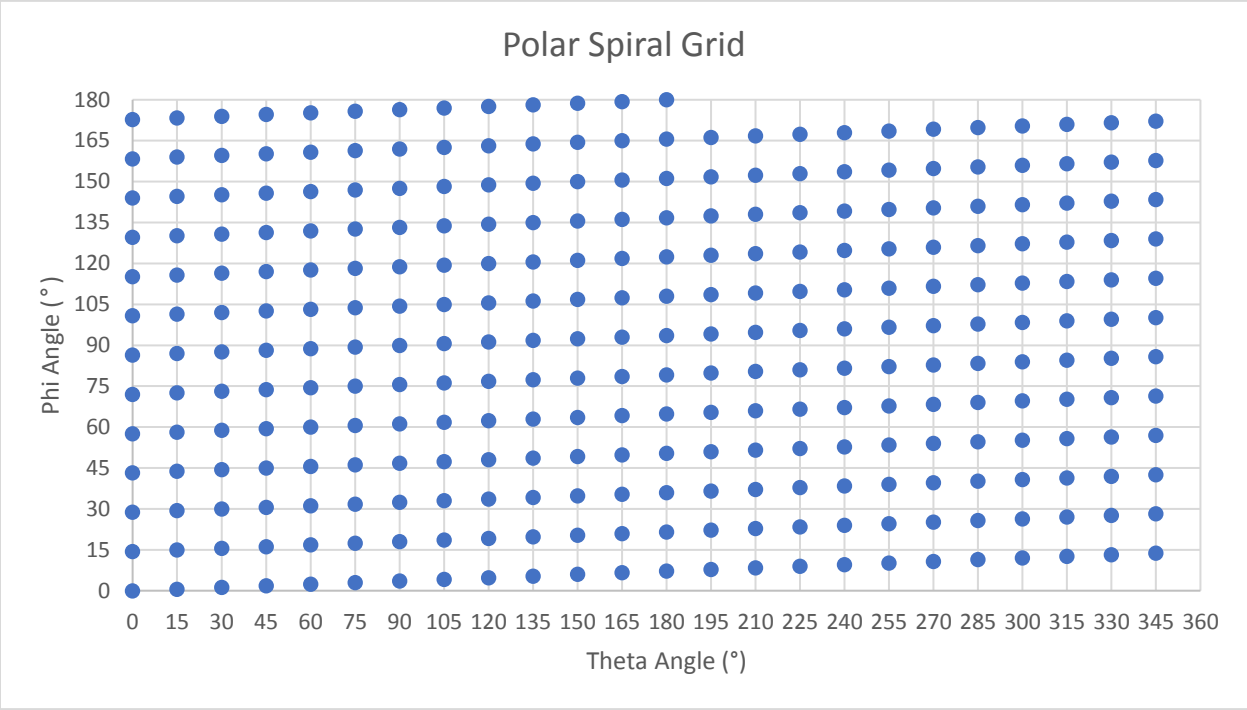

Figure 3.1.4-3 Sample Distribution of Measurement Grid Points in 2D for a Constant Velocity Polar Spiral Scan Grid with 301 Measurement Points

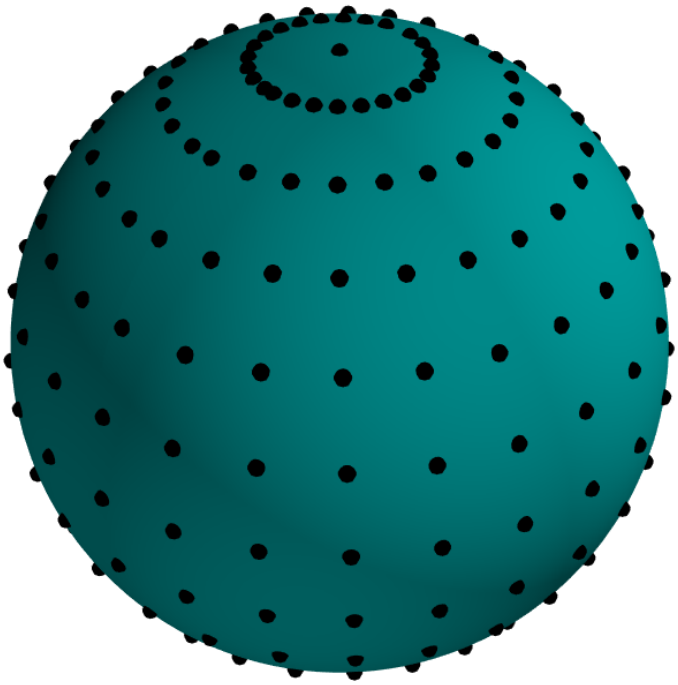

Figure 3.1.4-4 Sample Distribution of Measurement Grid Points in 3D for a Constant Velocity Polar Spiral Scan Grid with 301 Measurement Points

The polar spiral grid also has the advantage that minor differences in the ratios between theta and phi angles can result in pseudo-random positions resembling that of a constant density grid, but still with higher density near the poles.

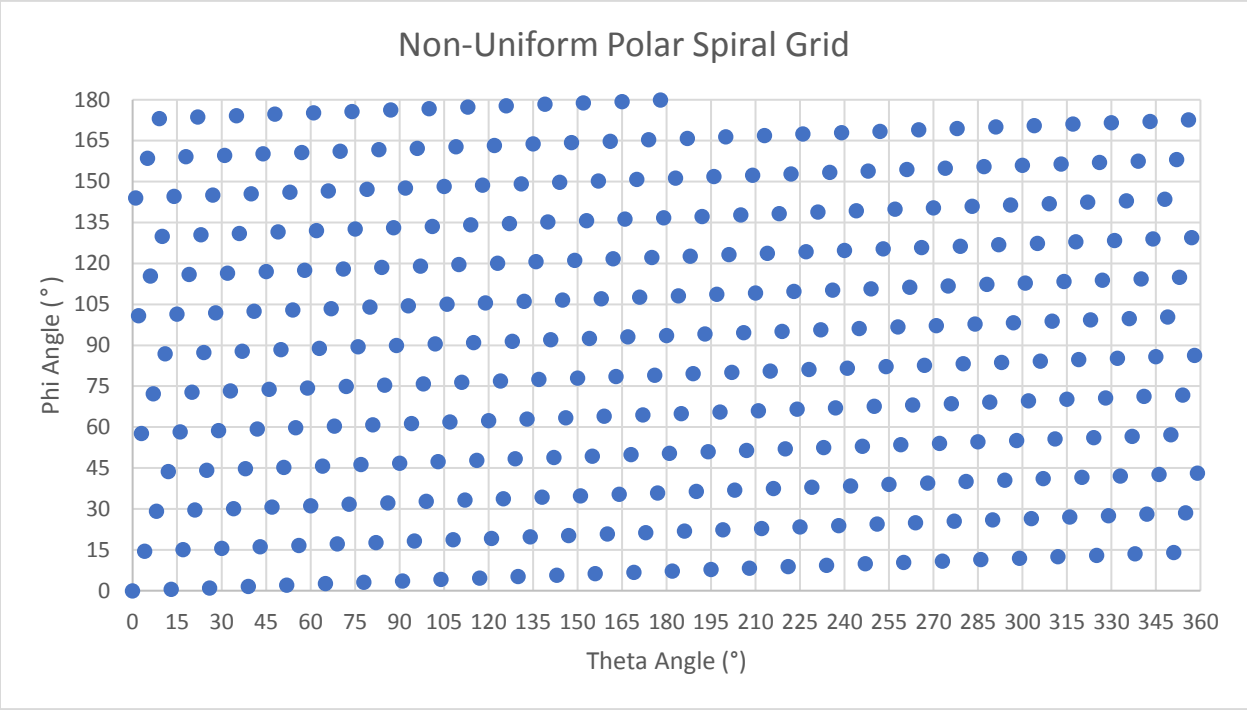

Figure 3.1.4-5 Sample Distribution of Measurement Grid Points in 2D for a Constant Velocity Polar Spiral Scan Grid with 361 Unique Measurement Points

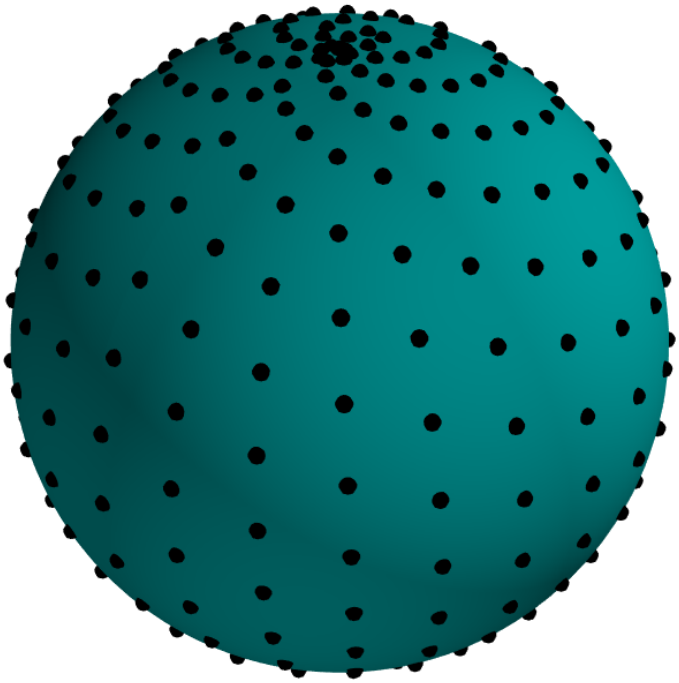

Figure 3.1.4-6 Sample Distribution of Measurement Grid Points in 2D for a Constant Velocity Polar Spiral Scan Grid with 361 Unique Measurement Points

3.1.5 Polar Limitations

As illustrated in Figure 3.1.5-1 for systems that either do not allow measurements at the pole ($\theta = 180°$), e.g., using distributed-axes positioners, or systems that have the positioners/support structures block the radiation towards the pole $\theta = 180°$), e.g., combined-axes positioners, the measurements in the region close to the pole at $\theta = 180°$ can be skipped and interpolated instead.

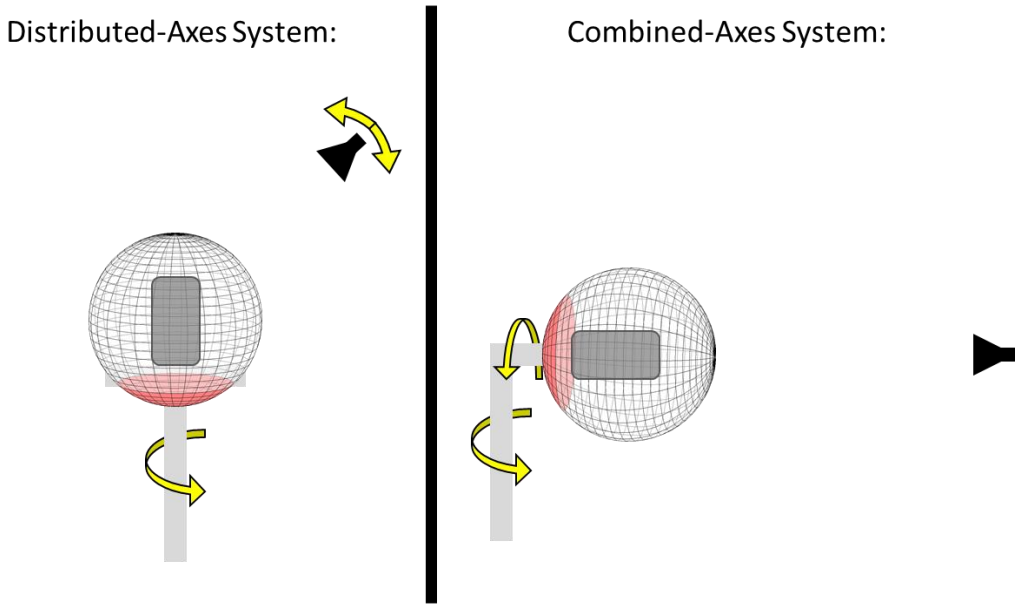

Figure 3.1.5-1 Illustration of Areas Around the Pole That Either Cannot be Reached by the Measurement Antenna or are Blocked by the Positioner

3.2 Spatial Averaging

The spatially averaged effective radiated power and sensitivity values are derived from the measurement data. The spatial average is calculated as a spherically weighted average over all measured data points. Figure B-1 illustrates one representation of the spherical surface area associated with each point on a constant (15 degree) angular step-size grid. It's apparent that for a given phi axis cut (i.e. a given theta value) that the area associated with each data point is the same, but that they vary as a function of theta. Thus, we can perform a uniformly weighted average of each point on a given phi cut, and then apply surface area weighting as a function of theta as shown in Figure 3.2-1. Note that the pole points at $\theta = 0°$ and $\theta = 180°$ degrees do have a surface area associated with them and thus do contribute to the spherically weighted average. The remaining cuts follow a sine-theta ($\sin(\theta)$) weighted behavior, but with a scaling factor related to the step size to address the small area associated with the poles. The resulting sum (average) still converges to the spherical integral equation at the infinitesimal limit, but for the relatively large step sizes used here, especially for TIS, the addition of the non-zero weighted pole points is necessary to minimize the overall error in the result.

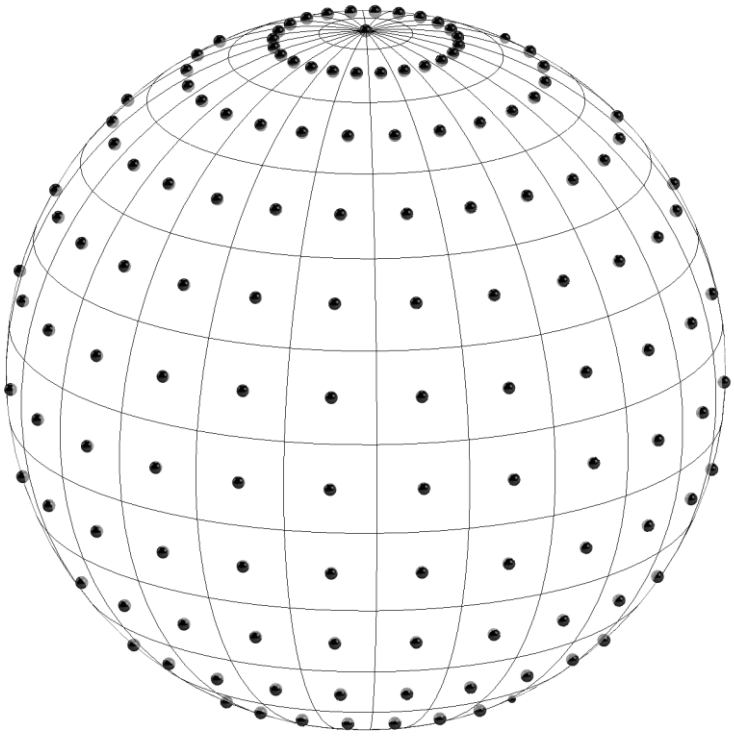

Figure 3.2-1 Illustration of the Spherical Surface Area Associated with Each Point on a Constant Angular Step-Size Grid

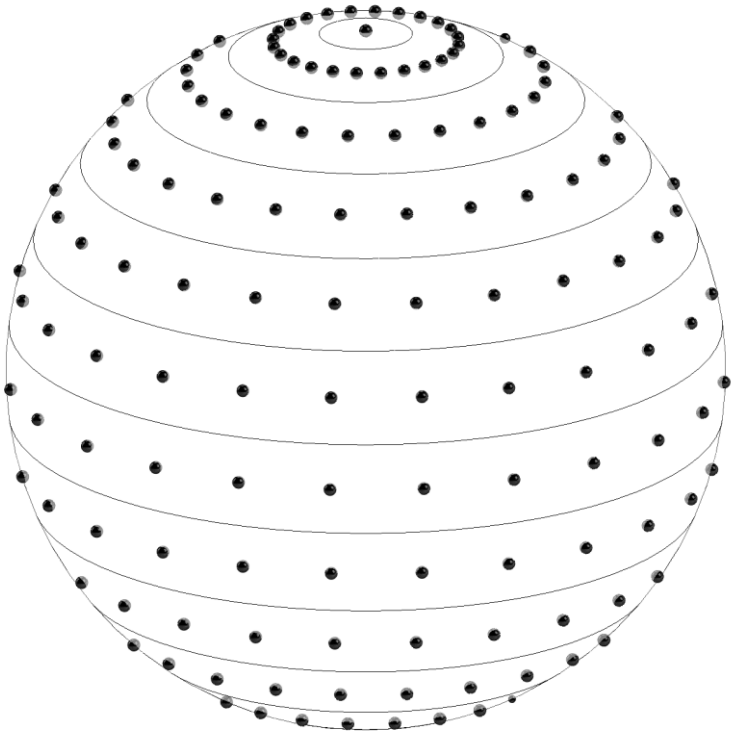

Figure 3.2-2 Illustration of the Spherical Surface Area Associated with Each Phi Cut on a Constant Angular Step-Size Grid

While the segmented spherical surface weighting provides an excellent approximation to the spherical integral for a low-resolution surface, the choice of surface segments evenly divided in theta is still arbitrary. Another approach uses the Clenshaw-Curtis (CLC) quadrature rule to integrate in theta. This approach uses some clever coordinate substitution to apply Lagrange polynomial fits to each average phi cut. The sinusoidal scaling of the resulting Chebyshev polynomial weighting functions causes the corresponding curve fit to show excellent correlation to smoothly varying sinusoid squared functions like those that make up spherical power patterns. By converting the Clenshaw-Curtis weights to equivalent surface weights, it's easy to see how CLC weighting differs from uniform surface segments (Figure 3.2-3), giving slightly less weight to the pole point and shifting all remaining segments closer to the pole. While the angular separation on the subsequent cuts gets slightly larger than the even step size, the actual area associated with the CLC weighting is smaller for the first couple of steps due to the proximity to the pole. Eventually, the CLC weighting becomes slightly higher than the evenly spaced weighting for each cut. While Clenshaw-Curtis weights can only be calculated for a full surface of phi-cuts evenly spaced in theta, using the spherical surface weight conversion for each CLC weight allows for proper computation of partial surface metrics as well.

.

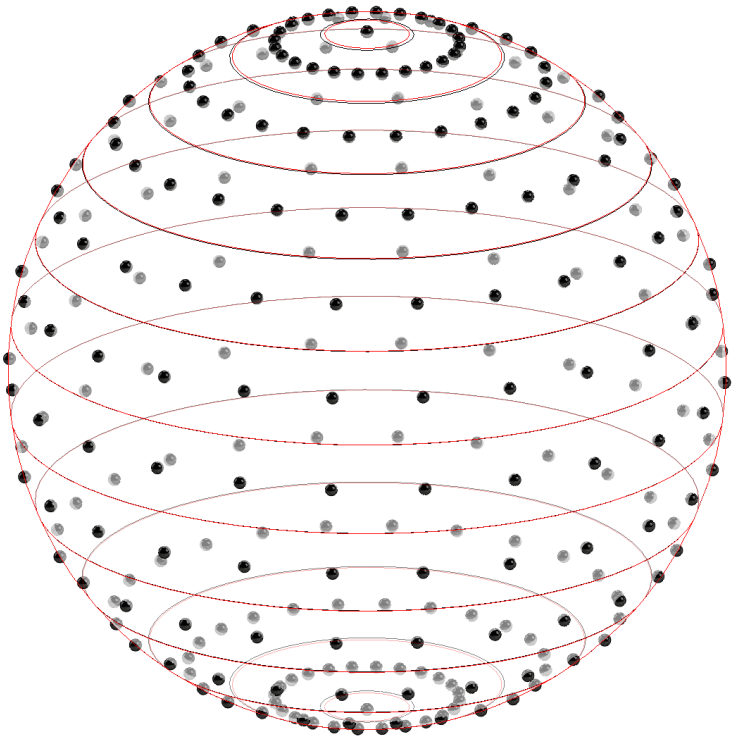

Figure 3.2-3 Overlay of 15-degree Surface Segments (Black Borders) with Clenshaw-Curtis Surface Segments (Red Borders), Showing the Dividing Conical Cuts Being Slightly Smaller on the Segments Near the Poles

For theta dependent phi grids, the point spacing varies in phi, while the theta spacing remains constant. Thus, while the surface area per point changes to something closer to constant, the surface area per cut remains the same as for the constant angular step size grid and thus the Clenshaw-Curtis weighting must still be applied to the average of each cut. Likewise, the partial surface metrics are easily computed from this same data.

For the constant density grid, each measured data point is assumed to be associated with the same amount of area and thus the weights for all points are one (constant). Therefore, the spatial average is simply the average of all measured points. However, the actual portion of the spherical surface associated with each measured data point is arbitrary and undefined, so there is currently no way to determine what portion of the surface associated with a given data point is intersected by the boundary of a partial surface segment. This implies that partial surface metrics cannot easily be computed accurately from the constant density grid data and therefore test methods that require the partial surface metrics cannot be measured using the constant density grid.

In the subsequent sections, *N* and *M* define the number of angular intervals in theta and phi, respectively. Note that *N* and *M* are different for the transmit and receive measurements. N and M for the TRP and TIS measurement grids outlined in Table 3.1-1 and 4.1-1 of *CTIA 01.20* [6] respectively, are tabulated in Table 3.2-1. Selecting finer measurement grids is not precluded. In both cases, the respective theta and phi indices, *i* and *j*, correspond to the measurement angles as demonstrated in Table RA.2-1 and Table RA.2-2 located in *CTIA 01.03* [5]. A complete definition of terms is given Section 2.

Table 3.2-1: Number of Angular Intervals *N* and *M*

Applicability Condition	*N*, *M*, $\Delta\theta$	Transmit Tests		Receive Tests	
		Minimum	Alternate	Minimum	Alternate
Below 3 GHz and Device Size ≤ 30 cm	*N*	6	12	4	6
	M	12	24	8	12
	$\Delta\theta$ [°]	30	15	45	30
Below 3 GHz and Device Size > 30 cm	*N*	12	NA	6	NA
	M	24	NA	12	NA
	$\Delta\theta$ [°]	15	NA	30	NA
Above 3 GHz	*N*	12	NA	6	NA
	M	24	NA	12	NA
	$\Delta\theta$ [°]	15	NA	30	NA
Note 1: For LBS technologies, the measurement grids should use $\Delta\theta$=30° .					

When the measurement has been made based on RSS values, the spatially averaged quantities have to be calculated according to the guidelines given in Section 2.1.1 using the linearized RSS values and the sensitivity search result.

Although the pattern data (EIRP and EIS quantities) are reported in units of dBm, the data is to be converted to linear units of milliwatts (mW) to perform the calculations in this section.

3.3 Total Radiated Power

For a complete sphere measured with N theta intervals and M phi intervals, both with even angular spacing, the Total Radiated Power is calculated as follows.

Total Radiated Power:

Equation 3.3-1

$$TRP \cong \frac{1}{2}\sum_{i=0}^{N} w_i \, cut_i$$

where

Equation 3.3-2

$$cut_i = \frac{1}{M}\sum_{j=0}^{M-1}\left[EIRP_\theta(\theta_i,\phi_j) + EIRP_\phi(\theta_i,\phi_j)\right]$$

is the average power for the phi cut at each theta angle (including the poles at index 0 and N if needed), and

Equation 3.3-3

$$w_i = \frac{c_i}{N}\left[1 - \sum_{j=1}^{\mathrm{int}(\frac{N}{2})}\frac{b_j}{4j^2-1}\cos(2j\theta_i)\right]$$

is the Clenshaw-Curtis weighting factor, with

$$b_j = \begin{cases} 1, & 2j = N \\ 2, & \text{otherwise} \end{cases}$$

and

$$c_i = \begin{cases} 1, & i = 0 \text{ or } N \\ 2, & \text{otherwise} \end{cases}$$

3.3.1 Theta Dependent Phi TRP

For the theta dependent phi optimization, where the number of phi intervals, M_i, is a function of the theta angle, the average power for each phi cut is calculated as follows:

Equation 3.3.1-1

$$cut_i = \frac{1}{M_i}\sum_{j=0}^{M_i-1}\left[EIRP_\theta(\theta_i,\phi_j) + EIRP_\phi(\theta_i,\phi_j)\right]$$

where:

$$M_i = N_\phi(\theta_i)$$

$$N_\phi(\theta) = 1 + int\left(\left(N_\phi(90^\circ) - 1\right)\sin(\theta)\right)$$

3.3.2 Spiral Scan TRP

When using the standard measurement grid, the sphere has N theta intervals and M phi intervals, both with even angular spacing. M and N are integers and the Total Radiated Power is calculated per Equation 3.3.2-1.

In the case of the spiral scan measurement grid, M and N need not be integers and can vary between measurements, but are nonetheless important in deriving the formulas for calculating TRP and other PRP figures.

The relationship between M, N, and the average step sizes in Theta and Phi are as follows:

Equation 3.3.2-1

$$M = \frac{2\pi}{\Delta\phi_{ave}}$$

Equation 3.3.2-2

$$N = \frac{\pi}{\Delta\theta_{ave} \cdot M}$$

where $\Delta\phi_{ave}$ is the average step size in phi, and $\Delta\theta_{ave}$ is the average step size in theta.

T or the total number of test points is approximately as follows:

Equation 3.3.2-3

$$T \approx M \cdot N = \frac{\pi}{\Delta\theta_{ave}}$$

The number T represents all test points including virtual test points (i.e., test points between $\theta = 165°$ and $\theta = 180°$ and/or $\theta = 0°$ and $\theta = 15°$ which must be extrapolated in some measurement systems).

In the case of the spiral measurement grid, points near a boundary interface must be used in calculating the power of areas proximate to the boundary. This typically involves all points within one rotation in phi from the interface boundary. It is therefore useful to define $M_{int,}$ an integer approximation of M as follows:

Equation 3.3.2-4

$$M_{int} = \text{int}\left[\frac{2\pi}{\Delta\phi_{ave}}\right]$$

The corresponding equation to Equation 3.3.2-1 when using a spiral grid of points to cover the sphere is given by Equation 3.3.2-5.

For the spiral scan TRP test method, the Total Radiated Power is calculated as follows:

Equation 3.3.2-5

$$TRP \approx \frac{\Delta\theta_{ave} \cdot [P_A + P_B + P_C]}{4 \cdot \Delta\phi_{ave}}$$

where:

P_A is the power contribution of area A (transition region 1).

P_B is the power contribution of area B (area without special weighting).

P_C is the power contribution of area C (transition region 2).

The exact formulas for P_A, P_B, and P_C depend on the types of regions to be calculated. When calculating TRP, the following values are used for P_A, P_B, and P_C:

Equation 3.3.2-6

$$P_A = \sum_{t=1}^{A-1} \left[EIRP_\theta(\theta_t, \phi_t) + EIRP_\phi(\theta_t, \phi_t)\right] \sin(\theta_t) \cdot [\phi_{t+1} - \phi_{t-1}] \cdot \left[\frac{1}{2}\right]$$

Equation 3.3.2-7

$$P_B = \sum_{t=A}^{B} \left[EIRP_\theta(\theta_t, \phi_t) + EIRP_\phi(\theta_t, \phi_t)\right] \sin(\theta_t) \cdot [\phi_{t+1} - \phi_{t-1}]$$

Equation 3.3.2-8

$$P_C = \sum_{t=B+1}^{T} \left[EIRP_\theta(\theta_t, \phi_t) + EIRP_\phi(\theta_t, \phi_t)\right] \sin(\theta_t) \cdot [\phi_{t+1} - \phi_{t-1}] \cdot \left[\frac{1}{2}\right]$$

where θ_t and ϕ_t are the theta and phi angles associated with test point t in the spiral scan test. M_{int} is defined in Equation 3.3.2-8.

A is defined as the test point which is one revolution in phi from the pole where one started measuring ($\theta = 0°$). B is the point at which the test point is an entire revolution from the final point at the end of the measurement ($\theta = 180°$). In some cases, A and/or B may be an extrapolated point as some measurement systems cannot measure to the point $\theta = 180°$. Note that $A \cong M_{int}$ and $B \cong T - M_{int}$ where T is the total number of measurement points.

This method assumes that $EIRP_\theta$ and $EIRP_\phi$ measurements are taken at the same location. If $EIRP_\theta$ and $EIRP_\phi$ are measured alternating using a single spiral cut or two spiral measurements are taken to measure $EIRP_\theta$ and $EIRP_\phi$ separately, then the sums in Equation 3.3.2-6 to Equation 3.3.2-8 should split for $EIRP_\theta$ and $EIRP_\phi$ as different angles are used for the different polarizations.

3.3.3 Constant Density Grid

For constant density grid types using the charged particle approach, the TRP integration should ideally use the area of the Voronoi region surrounding each grid point. Assuming an ideal constant density configuration of the grid points, the TRP can be approximated using

$$\text{TRP} \approx \frac{1}{N} \sum_{i=0}^{N-1} \left[\text{EIRP}_\theta(\theta_i, \phi_i) + \text{EIRP}_\phi(\theta_i, \phi_i)\right]$$

3.4 Near-Horizon Partial Radiated Power

Since the formulation for the Clenshaw-Curtis weights only works for a complete spherical surface ($\theta = 0$ to $180°$), an additional formulation is needed for the weighting of surface segments at the edge of a partial surface.

Equation 3.4-1

$$w_{partial\ segment} = \cos(\theta_{edge}) - 1 + \sum_{i=0}^{n_{edge}} w_i$$

where θ_{edge} is the angle of the edge of the partial surface and n_{edge} is the index of the surface segment containing that edge.

For a complete sphere measured with *N* = 6 theta intervals with even angular spacing, see Equation 3.4-2, the Near-Horizon Partial Radiated Power is calculated as follows. The power radiated over ±45 degrees near the horizon is given by:

Equation 3.4-2

$$NHPRP_{\pm 45} \cong \frac{1}{2}(w_{\pm 45}\ (cut_2 + cut_4) + w_3\ cut_3)$$

where

$$w_{\pm 45} = \cos(45°) - 1 + \sum_{i=0}^{2} w_i$$

and both w_i and cut_i maintain the same definitions as for TRP in Section 3.3.

For a complete sphere measured with *N* = 12 theta intervals with even angular spacing, see Equation 3.4-3, the Near-Horizon Partial Radiated Power is calculated as follows. The power radiated over ±45 degrees near the horizon is given by:

Equation 3.4-3

$$NHPRP_{\pm 45} \cong \frac{1}{2}\left(w_{\pm 45}\ (cut_3 + cut_9) + \sum_{i=4}^{8} w_i\ cut_i\right)$$

where

$$w_{\pm 45} = \cos(45°) - 1 + \sum_{i=0}^{3} w_i$$

3.4.1 Spiral Scan NHPRP

To calculate NHPRP using the spiral method, an equation similar to Equation 3.4 4 is used with slight modification to the terms P_A, P_B, and P_C:

Equation 3.4-4

$$NHPRP \approx \frac{\Delta\theta_{ave} \cdot |P_A + P_B + P_C|}{4 \cdot \Delta\phi_{ave}}$$

where points A and B are redefined as follows:

- A is the upper boundary point for the measurement region being calculated (for example, the point closest to $\theta = 45°$ for $NHPRP_{\pm 45}$)
- B is the lower boundary point for the region being calculated.

and where

P_A represents the transition area at the upper boundary of the NHPRP region,

P_B represents the area within the NHPRP region which is non-transitional,

P_C represents the transition area at the lower boundary of the NHPRP region,

$\Delta\phi_{ave}$ is the average step size in phi, and

$\Delta\theta_{ave}$ is the average step size in theta.

The equations for the contributions for NHPRP are as follows:

Equation 3.4-5

$$P_A = \sum_{t=A-M_{int}}^{A+M_{int}} \left[EIRP_\theta(\theta_t, \phi_t) + EIRP_\phi(\theta_t, \phi_t)\right] \sin(\theta_t) \cdot [\phi_{t+1} - \phi_{t-1}] \cdot \left[1 - \frac{(\theta_{A-M_{int}} - \theta_t)}{(\theta_{A+M_{int}} - \theta_{A-M_{int}})}\right]$$

Equation 3.4-6

$$P_B = \sum_{t=A+M_{int}+1}^{B-M_{int}-1} \left[EIRP_\theta(\theta_t,\phi_t) + EIRP_\phi(\theta_t,\phi_t)\right] \sin(\theta_t) \cdot [\phi_{t+1} - \phi_{t-1}]$$

Equation 3.4-7

$$P_C = \sum_{t=B-M_{int}}^{B+M_{int}} \left[EIRP_\theta(\theta_t,\phi_t) + EIRP_\phi(\theta_t,\phi_t)\right] \sin(\theta_t) \cdot [\phi_{t+1} - \phi_{t-1}] \cdot \left[1 - \frac{(\theta_t - \theta_{B-M_{int}})}{(\theta_{B+M_{int}} - \theta_{B-M_{int}})}\right]$$

where θ_t and ϕ_t are the theta and phi angles associated with test point t in the spiral scan test. M_{int} is defined in Equation 3.3.2-4.

This method assumes that EIRP$_\phi$ and EIRP$_\theta$ are taken at the same location. If EIRP$_\phi$ and $EIRP_\theta$ are measured alternating using a single spiral cut or two spiral measurements are taken to measure $EIRP_\phi$ and $EIRP_\theta$ separately, then the sums in Equation 3.4 5 to Equation 3.4 7 should split for $EIRP_\phi$ and $EIRP_\theta$ as different angles are used for the different polarizations.

3.5 Total Isotropic Sensitivity

For a complete sphere measured with *N* theta intervals and *M* phi intervals, both with even angular spacing, the Total Isotropic Sensitivity is calculated as follows.

Total Isotropic Sensitivity:

Equation 3.5-1

$$TIS \cong \left[\frac{1}{2}\sum_{i=0}^{N} w_i \, cut_i\right]^{-1}$$

where

$$cut_i = \frac{1}{M}\sum_{j=0}^{M-1}\left[\frac{1}{EIS_\theta(\theta_i,\phi_j)} + \frac{1}{EIS_\phi(\theta_i,\phi_j)}\right]$$

is the average for the conical phi cut at each theta angle (including the poles at index 0 and *N* if needed),

and

$$w_i = \frac{c_i}{N}\left[1 - \sum_{j=1}^{\mathrm{int}(\frac{N}{2})}\frac{b_j}{4j^2-1}\cos(2j\theta_i)\right]$$

is the Clenshaw-Curtis weighting factor, with

$$b_j = \begin{cases} 1, & 2j = N \\ 2, & otherwise \end{cases}$$

and

$$c_i = \begin{cases} 1, & i = 0\ or\ N \\ 2, & otherwise \end{cases}$$

and where EIS is the radiated effective isotropic sensitivity measured at each direction and polarization.

3.5.1 Theta Dependent Phi TIS

For the theta dependent phi optimization, where the number of phi intervals, M_i, is a function of the theta angle, the average for each cut is calculated as follows:

Equation 3.5-2

$$cut_i = \frac{1}{M_i}\sum_{j=0}^{M_i-1}\left[\frac{1}{EIS_\theta(\theta_i,\phi_j)} + \frac{1}{EIS_\phi(\theta_i,\phi_j)}\right]$$

3.6 Near-Horizon Partial Isotropic Sensitivity

For a complete sphere measured with *N* = 4 theta intervals and *M* phi intervals, see Equation 3.6-1, both with even angular spacing, the Near-Horizon Partial Isotropic Sensitivity is calculated as follows.

For sensitivity considered over ±45 degrees near the horizon, the result is given by:

Equation 3.6-1

$$NHPIS_{\pm 45} \cong \left[\frac{1}{2}\left(w_{\pm 45}\,(cut_1 + cut_3) + w_2\,cut_2\right)\right]^{-1}$$

where

$$w_{\pm 45} = \cos(45°) - 1 + \sum_{i=0}^{1} w_i$$

and both w_i and cut_i maintain the same definitions as for TIS in Section 3.5.

For a complete sphere measured with *N* = 6 theta intervals and *M* phi intervals, see Equation 3.6-2, both with even angular spacing, the Near-Horizon Partial Isotropic Sensitivity is calculated as follows. For sensitivity considered over ±45 degrees near the horizon, the result is given by:

Equation 3.6-2

$$NHPIS_{\pm 45} \cong \left[\frac{1}{2}\left(w_{\pm 45}\,(cut_2 + cut_4) + w_3\,cut_3\right)\right]^{-1}$$

where

$$w_{\pm 45} = \cos(45°) - 1 + \sum_{i=0}^{2} w_i$$

3.7 Upper Hemisphere Isotropic Sensitivity (UHIS)

For a complete sphere measured with *N* = 4 theta intervals with even angular spacing, see Equation 3.7-1, the Upper Hemisphere Isotropic Sensitivity, which represents the total power radiated in the theta range from 0 to 90 degrees is calculated as follows.

Equation 3.7-1

$$UHIS \cong \left[\frac{1}{2}\left(\sum_{i=0}^{1} w_i\,cut_i + \frac{w_2\,cut_2}{2}\right)\right]^{-1}$$

where w_i and cut_i maintain the same definitions as for TIS in Section 3.5.

For a complete sphere measured with *N* = 6 theta intervals with even angular spacing, see Equation 3.7-2, the Upper Hemisphere Isotropic Sensitivity, which represents the total power radiated in the theta range from 0 to 90 degrees is calculated as follows.

Equation 3.7-2

$$UHIS \cong \left[\frac{1}{2}\left(\sum_{i=0}^{2} w_i \, cut_i + \frac{w_3 \, cut_3}{2}\right)\right]^{-1}$$

3.8 Partial Isotropic GNSS Sensitivity (PIGS)

For a complete sphere measured with *N* = 4 theta intervals with even angular spacing, see Equation 3.8-1, the Partial Isotropic GNSS Sensitivity, which represents the total power radiated in the theta range from 0 to 120 degrees is calculated as follows:

Equation 3.8-1

$$PIGS \cong \left[\frac{1}{2}\left(w_{\pm 30} \, cut_2 + \sum_{i=0}^{1} w_i \, cut_i\right)\right]^{-1}$$

where w_i and cut_i maintain the same definitions as for TIS in Section 3.5 and where

$$w_{\pm 30} = \cos(60°) - 1 + \sum_{i=0}^{1} w_i$$

For a complete sphere measured with *N* = 6 theta intervals with even angular spacing, see Equation 3.8-2, the Partial Isotropic GNSS Sensitivity, which represents the total power radiated in the theta range from 0 to 120 degrees is calculated as follows:

Equation 3.8-2

$$PIGS \cong \left[\frac{1}{2}\left(w_{\pm 30} \, cut_4 + \sum_{i=0}^{3} w_i \, cut_i\right)\right]^{-1}$$

where w_i and cut_i maintain the same definitions as for TIS in Section 3.5 and where

$$w_{\pm 30} = \cos(60°) - 1 + \sum_{i=0}^{2} w_i$$

3.9 Average 3D C/N_0

For a complete sphere measured with *N* theta intervals and *M* phi intervals, both with even angular spacing, the Average 3D C/N_0 is calculated as follows.

Average 3D C/N$_0$:

Equation 3.9-1

$$3D\_CN0_{avg} \cong \frac{1}{2}\sum_{i=0}^{N} w_i \, cut_i$$

where

$$cut_i = \frac{1}{M}\sum_{j=0}^{M-1}\left[CN0_\theta(\theta_i,\phi_j) + CN0_\phi(\theta_i,\phi_j)\right]$$

is the average C/N$_0$ for the phi cut at each theta angle (including the poles at index 0 and *N* if needed), w_i is the Clenshaw-Curtis weighting factor as defined in Equation 3.3-3, and $CN0$ is the linearized C/N$_0$ measured at each direction and polarization in linear units.

3.10 Theta Dependent Phi Average 3D C/N$_0$

For a complete sphere measured with *N* theta intervals and *M* phi intervals, both with even angular spacing, the Average 3D C/N$_0$ is calculated as follows.

For the Theta Dependent Phi Optimization, where the number of phi intervals, M_i, is a function of the theta angle, the Average 3D C/N$_0$ for each phi cut is calculated as follows:

Equation 3.10-1

$$cut_i = \frac{1}{M_i}\sum_{j=0}^{M_i-1}\left[CN0_\theta(\theta_i,\phi_j) + CN0_\phi(\theta_i,\phi_j)\right]$$

where $M_i = N_\phi(\theta_i)$ and $CN0$ is the linearized C/N$_0$ measured at each direction and polarization.

3.11 Upper Hemisphere 3D C/N$_0$

For a complete sphere measured with $N = 6$ theta intervals with even angular spacing, the Upper Hemisphere 3D C/N$_0$ ($3D\_CN0_{UH}$), which is the C/N$_0$ integrated over the upper hemisphere (theta range from 0 to 90 degrees), is calculated as follows.

Equation 3.11-1

$$3D\_CN0_{UH} \cong \frac{1}{2}\left(\sum_{i=0}^{2} w_i\, cut_i + \frac{w_3\, cut_3}{2}\right)$$

where w_i and cut_i maintain the same definitions as for Average 3D C/N$_0$ in Section 3.9.

For a complete sphere measured with $N = 4$ theta intervals with even angular spacing, the Upper Hemisphere 3D C/N$_0$ ($3D\_CN0_{UH}$), which is the C/N$_0$ integrated over the upper hemisphere (theta range from 0 to 90 degrees), is calculated as follows.

Equation 3.11-2

$$3D\_CN0_{UH} \cong \frac{1}{2}\left(\sum_{i=0}^{1} w_i\, cut_i + \frac{w_2\, cut_2}{2}\right)$$

3.12 Partial Isotropic GNSS Hemisphere 3D C/N$_0$

For a complete sphere measured with $N = 6$ theta intervals (30 degree spacing) with even angular spacing, the Partial Isotropic GNSS 3D C/N$_0$ ($3D\_CN0_{PIG}$), which is the C/N$_0$ integrated over the theta range from 0 to 120 degrees, is calculated as follows:

Equation 3.12-1

$$3D\_CN0_{PIG} \cong \frac{1}{2}\left(w_{\pm 30}\, cut_4 + \sum_{i=0}^{3} w_i\, cut_i\right)$$

where w_i and cut_i maintain the same definitions as for Average 3D C/N$_0$ in Section 3.9 and where

$$w_{\pm 30} = \cos(60°) - 1 + \sum_{i=0}^{2} w_i$$

For a complete sphere measured with $N = 4$ theta intervals (45 degree spacing) with even angular spacing, the Partial Isotropic GNSS 3D C/N$_0$ ($3D\_CN0_{PIG}$), which is the C/N$_0$ integrated over the theta range from 0 to 120 degrees, is calculated as follows:

Equation 3.12-2

$$3D\_CN0_{PIG} \cong \frac{1}{2}\left(w_{\pm 30}\, cut_2 + \sum_{i=0}^{1} w_i\, cut_i\right)$$

where w_i and cut_i maintain the same definitions as for Average 3D C/N$_0$ in Section 3.9 and where

$$w_{\pm 30} = \cos(60°) - 1 + \sum_{i=0}^{1} w_i$$

Section 4 Symmetry Pattern Antenna

The pattern symmetry requirement specified in *CTIA 01.20* [5] should not be misinterpreted as an absolute accuracy requirement. A requirement of ±0.1 dB for antenna pattern measurements taken in the cellular and PCS bands would be very challenging to accomplish. To clarify pattern symmetry, and provide context for selecting its value, the following is provided for informational purposes only.

4.1 Symmetry Pattern vs. Absolute Accuracy

The expanded uncertainty budget required by this test plan is cited in *CTIA 01.20* [5]. Given this specification, consideration must be given to the many items in the complete uncertainty budget that contribute to this final total. Examples of these are the uncertainty of the instrument used to measure absolute power (e.g., spectrum analyzer or power meter), the uncertainty with which the gain of the calibrated reference antenna was measured, quiet zone accuracy (i.e., ripple or reflection in the chamber), etc. Many of these uncertainty contributions can be made quite small at these frequency ranges. Three-dimensional pattern integration of the calibrated reference antenna can yield very precise directivity references. In the case of measuring highly non-directive devices, the two largest single contributors to the uncertainty budget are usually the ultimate accuracy of the power measurement instrument, and the quiet zone accuracy (ripple) in the anechoic chamber.

To obtain the overall uncertainty desired, it is likely that a quiet zone ripple substantially better than ±1.0 dB is required. To quantify the quiet zone accuracy, an antenna (i.e., the omni-directional dipole or loop source) substantially better than the ±1.0 dB ripple level discerned, therefore, should be used. Thus, the omni-directional test antennas used for the chamber evaluation given in *CTIA 01.70* [7] (not necessarily for the range reference measurement in *CTIA 01.73* [8]) are required to have patterns that are symmetric to ±0.1 dB. This level of pattern symmetry is achieved rather easily with an electric dipole rotated about its axis, and can be achieved with some care with the uniform-current (Alford) loops described in this section. (Reference can also be made to *Loop Antennas with Uniform Current* [9].

Pattern symmetry is measured with an antenna centered precisely on the azimuth axis of rotation of the positioner. An anechoic chamber with a very low reflectivity is not required to verify a nominally omni-directional antenna's pattern symmetry. If an antenna with a perfectly symmetric omni pattern is precisely on the center of rotation, even if there is a substantial reflector in the chamber, a perfectly uniform pattern can be observed. This is because the signals on both the direct and reflected paths remain constant as the antenna is rotated. So, as long as an “omni” antenna starts out more or less omni, it can be qualified for pattern symmetry in a chamber that might not meet even the ±1.0 dB quiet zone ripple referred to above.

It is important to note this specification calls for pattern SYMMETRY of ±0.1 dB -- NOT absolute gain accuracy. In fact, for the chamber evaluation detailed in *CTIA 01.70* [7] (not the range reference measurement) phase, gain is not needed at all—only verification of the pattern symmetry. Furthermore, the ±0.1 dB symmetry requirement is not arbitrary; it follows directly from the desire to meet the expanded uncertainty budgets cited in *CTIA 01.20* [6].

To summarize, this specification does not require chamber evaluation antennas with a gain accuracy of ±0.1 dB. Rather, the antenna pattern symmetry should be ±0.1 dB, which is achievable and quantifiable.

Section 5 Path Loss Errors Induced by Propagation Delay

5.1 Description and Overview

Most traditional Network Analyzer (either Scalar or Vector) and Spectrum Analyzer / Tracking Generator measurements are made with short cables. In an OTA chamber there is significant propagation delay from the source to the receiver, due to the long cable lengths as well as the over-the-air path length. When swept measurements are made, by the time the signal travels from the source to the receiver, the instrument will be tuned to a higher frequency. This will result in an amplitude error that is a product of the (generally Gaussian) bandwidth filter response curve in (dB/Hz), the sweep rate in (Hz/s), and the propagation delay in (s).

There may be additional factors for particular instruments due to settling time issues if the synthesizer re-locks, or if the instrument performs other housekeeping, during the sweep.

Although list-based network analyzer measurements theoretically ought not exhibit this same phenomenon, propagation delay error is still possible depending on the combination of cable length, path loss length, instrument bandwidth, instrument settling time and instrument sampling time.

In general, the means of mitigating this problem for swept-based measurements is to slow down the sweep speed. In general, the means of mitigating this problem for list-based measurements is to delay the measurement sampling time (which may require an increase in the dwell time).

Discrete signal generator and receiver combinations are not subject to this phenomenon. As such, this discrete topology provides the most accurate verification for swept and list-based instrument configurations.

5.2 Verification Principles

Problems with swept measurements can typically be identified by slowing the sweep speed and watching for an increase in the measured signal (reduction in path loss). Depending on the particular instrument's coupling between IF Bandwidth and Sweep Time, reducing the IF Bandwidth may be used to identify this phenomenon. The result can be assumed to be valid when further adjustment of the settings causes no further increase in the measured signal level.

Problems with list-based measurements can typically be identified by delaying the measurement sampling time and watching for an increase in the measured signal (reduction in path loss). The result can be assumed to be valid when further adjustment of the settings causes no further increase in the measured signal level.

For both swept and list-based measurements the result is determined to be valid when the path loss at a given frequency when measured in the swept or list mode and the path loss at the same frequency when measured in the CW mode are within the repeatability of the instrumentation.

5.3 Continuous Wave Verification Procedure

A set of continuous wave (CW) measurements is made and compared to the automated swept or list-based measurements. The CW tests specifically utilize the procedures described in *Ancillary Procedures*. The respective steps a. and b. of these clauses describe vector and scalar measurement procedures.

For instrument sweeps or spans that encompass multiple dipole frequencies, it is recommended that CW measurements be performed at the center frequency of each of three reference dipoles (the lowest frequency dipole, the dipole nearest the mid-frequency of the sweep and the highest frequency dipole). For instrument sweeps or spans that encompass only one dipole frequency range, it is recommended that CW measurements be performed at the low, center and high frequencies of the dipole.

The CW measurements are performed in one configuration then compared with the results of the corresponding swept or list-based measurement(s) in the same configuration. Following are relevant conditions:

- The overall cable lengths for all configurations (combination of theta/phi polarization and TRP/TIS path) are approximately the same.
- The CW measurements utilize the same instrument settings as the swept or list-based measurements.
- The CW measurements use the same type of Calibration (Normalization / Full 2-port, etc. as chosen) as the swept or list-based measurements.
- The CW measurements are performed manually and the swept or list-based measurements are performed either manually or with the system software (as chosen).

If there is a significant difference in the various (theta/phi/TRP/TIS) path lengths then it is recommended to make measurements over the longest path; shorter lengths can be considered for additional verification.

Generally, verification only needs to be performed once for a particular combination of chamber model, coax cable length, instrument model and instrument settings.

Section 6 Test Channel Selection Guidelines for LTE CA OTA Testing

6.1 Purpose

This section describes the various guidelines used in selecting channels for CA combinations. These guidelines are not normative but should be useful in identifying test channels for new CA combinations.

6.2 Examples

These examples are excerpted from tables in *CTIA 01.50* [10] Section 4.

Example 1 (2 CA Inter-Band TRP): In this example channel 2450 is chosen is maximize the span between the PCC under test and the SCC.

CA_2A-5A	2	5	10	10	18650	2450	12 RB with RBstart=0	N/A	N/A
			10	10	18900	2450	12 RB with RBstart=19	N/A	N/A
			10	10	19150	2450	12 RB with RBstart=38	N/A	N/A

Example 2 (3 CA Inter-Band TRP): In this example, the SCC's are chosen to maximize the span since the PCC band falls between the SCC bands.

CA_2A-4A-5A	2	SCC1=4 SCC2=5	10	SCC1=10 SCC2=10	18650	SCC1=2350 SCC2=2450	12 RB with RBstart=0	N/A	N/A
					18900	SCC1=2350 SCC2=2450	12 RB with RBstart=19	N/A	N/A
					19150	SCC1=2350 SCC2=2450	12 RB with RBstart=38	N/A	N/A

Example 3 (3 CA Inter-Band TRP): In this example, SCC2 is chosen to maximize the span between the PCC under test and SCC2. The band for SCC1 falls in between the PCC band and the SCC2 band making the selection of the SCC1 channel arbitrary. In this example, the SCC1 was chosen to force the antenna to tune across the entirety of bands 2 and 4.

CA_13A-2A-4A	13	CA_13A-2A-4A	10	SCC1=10 SCC2=10	23230	SCC1=650 SCC2=2350	12 RB with RBstart=0	N/A	N/A
					23230	SCC1=650 SCC2=2350	12 RB with RBstart=19	N/A	N/A
					23230	SCC1=650 SCC2=2350	12 RB with RBstart=38	N/A	N/A

Example 4 (3 CA Inter-Band TRP): In this example, SCC2 is chosen to maximize the span between the PCC under test and SCC2. The band for SCC1 falls in between the PCC band and the SCC2 band making the selection of the SCC1 channel arbitrary. In this example, the SCC1 was chosen to force the antenna to tune across the entirety of band 4.

CA_13A-4A-4A	13	SCC1=4 SCC2=4	10	SCC1=10 SCC2=10	23230	SCC1=2000 SCC2=2350	12 RB with RBstart=0	N/A	N/A
					23230	SCC1=2000 SCC2=2350	12 RB with RBstart=19	N/A	N/A
					23230	SCC1=2000 SCC2=2350	12 RB with RBstart=38	N/A	N/A

Example 5 (3 CA Inter-Band TRP): In this example, SCC1 and SCC2 are chosen to maximize the span between the PCC under test and the intra-band, contiguous combination of SCC1 and SCC2.

CA_2A-66C	2	SCC1=66 SCC2=66	10	SCC1=10 SCC2=20	18650	SCC1=67086 SCC2=67230	12 RB with RBstart=0	N/A	N/A
					18900	SCC1=67086 SCC2=67230	12 RB with RBstart=19	N/A	N/A
					19150	SCC1=67086 SCC2=67230	12 RB with RBstart=38	N/A	N/A

For CA TRP where the PCC and SCC/SCC1 are intra-band, non-contiguous carriers, the following general rule was applied:

Table 6.2-1 CA TRP where the PCC and SCC/SCC1 are Intra-Band

PCC	SCC or SCC1
Low Channel	Mid Channel
Mid Channel	High Channel
High Channel	Low Channel

Example 6 (2 CA Intra-Band, Non-Contiguous TRP): In this example, the PCC and SCC channels are chosen based on the rule above in Table 6.2-1.

CA_4A-4A	4	4	10	10	20000	2175	12 RB with RBstart=0	N/A	N/A
			10	10	20175	2350	12 RB with RBstart=19	N/A	N/A
			10	10	20350	2000	12 RB with RBstart=38	N/A	N/A

Example 7 (3 CA with Intra-Band, Non-Contiguous component TRP): In this example, the PCC and SCC1 follow the rule above in Table 6.2-1 and the SCC2 is chosen to maximize the frequency span.

CA_4A-4A-5A	4	SCC1=4 SCC2=5	10	SCC1=10 SCC2=10	20000	SCC1=2175 SCC2=2450	12 RB with RBstart=0	N/A	N/A
					20175	SCC1=2350 SCC2=2450	12 RB with RBstart=19	N/A	N/A
					20350	SCC1=2000 SCC2=2450	12 RB with RBstart=38	N/A	N/A

For CA TRP where the PCC and SCC/SCC1 are intra-band, contiguous carriers, the following general rule was applied:

Table 6.2-2 CA TRP Where the PCC and SCC/SCC1 are Intra-Band

PCC	SCC or SCC1
Low Channel	Low Channel + One Channel
Mid Channel	Mid Channel +/- One Channel
High Channel	High Channel - One Channel

Example 8 (2 CA Intra-Band, Contiguous TRP): In this example, the PCC and SCC channels are chosen based on the rule above in Table 6.2-2.

CA_41C	41	41	20	20	39750	39948	18 RB with RBstart=0	N/A	N/A
			20	20	40620	40422	18 RB with RBstart=41	N/A	N/A
			20	20	41490	41292	18 RB with RBstart=82	N/A	N/A

For CA TIS, the SCC (or SCC's) were generally chosen based on the following rule:

Table 6.2-3 CA TIS

PCC	SCC or SCC1	SCC2 (for 3 CA)
Low Channel	Low Channel	Low Channel
Mid Channel	Mid Channel	Mid Channel
High Channel	High Channel	High Channel

Example 9 (2 CA Inter-Band TIS): In this example, the SCC is chosen based on the rule above in Table 6.2-3.

CA_2A-5A	2	5	10	10	650	2450	50 RB with RBstart=0	50 RB with RBstart=0	50 RB with RBstart=0
					900	2525	50 RB with RBstart=0	50 RB with RBstart=0	50 RB with RBstart=0
					1150	2600	50 RB with RBstart=0	50 RB with RBstart=0	50 RB with RBstart=0

Example 10 (3 CA Inter-Band TIS): In this example, the SCC1 and SCC2 are chosen based on the rule above in Table 6.2 3.

CA_2A-4A-5A	2	SCC1=4 SCC2=5	10	SCC1=10 SCC2=10	650	SCC1=2000	50 RB with RBstart=0	50 RB with RBstart=0	50 RB with RBstart=0	50 RB with RBstart=0
						SCC2=2450				
					900	SCC1=2175	50 RB with RBstart=0	50 RB with RBstart=0	50 RB with RBstart=0	50 RB with RBstart=0
						SCC2=2525				
					1150	SCC1=2350	50 RB with RBstart=0	50 RB with RBstart=0	50 RB with RBstart=0	50 RB with RBstart=0
						SCC2=2600		50 RB with RBstart=0	50 RB with RBstart=0	50 RB with RBstart=0

For CA TIS where the PCC and SCC/SCC1 are intra-band, non-contiguous carriers, the same general rule was applied as in TRP in Table 6.2-1.

Example 11 (2 CA Intra-Band, Non-Contiguous TIS): In this example, the PCC and SCC channels are chosen based on the same rule as TRP using Table 6.2-1.

CA_4A-4A	4	4	10	10	2000	2175	50 RB with RBstart=0	50 RB with RBstart=0	50 RB with RBstart=0
					2175	2350	50 RB with RBstart=0	50 RB with RBstart=0	50 RB with RBstart=0
					2350	2000	50 RB with RBstart=0	50 RB with RBstart=0	50 RB with RBstart=0

Example 12 (3 CA with Intra-Band, Non-Contiguous component TIS): In this example, the PCC and SCC1 follow the rule in Table 6.2-1 while SCC2 is chosen based on Table 6.2-3.

CA_4A-4A-5A	4	SCC1=4 SCC2=5	10	SCC1=10 SCC2=10	2000	SCC1=2175 SCC2=2450	50 RB with RBstart=0	50 RB with RBstart=0	50 RB with RBstart=0	50 RB with RBstart=0
					2175	SCC1=2350 SCC2=2525	50 RB with RBstart=0	50 RB with RBstart=0	50 RB with RBstart=0	50 RB with RBstart=0
					2350	SCC1=2000 SCC2=2600	50 RB with RBstart=0	50 RB with RBstart=0	50 RB with RBstart=0	50 RB with RBstart=0

Example 13 (3 CA with Intra-Band, Non-Contiguous component TIS): In this example, the intra-band, non-contiguous SCC1 and SCC2 follow the rule in Table 6.2-1 while the PCC is chosen based on Table 6.2-3.

CA_5A-4A-4A	5	SCC1=4 SCC2=4	10	SCC1=10 SCC2=10	2450	SCC1=2000 SCC2=2175	25 RB with RBstart=25	50 RB with RBstart=0	50 RB with RBstart=0	50 RB with RBstart=0
					2525	SCC1=2175 SCC2=2350	25 RB with RBstart=25	50 RB with RBstart=0	50 RB with RBstart=0	50 RB with RBstart=0
					2600	SCC1=2350 SCC2=2000	25 RB with RBstart=25	50 RB with RBstart=0	50 RB with RBstart=0	50 RB with RBstart=0

For CA TIS where the PCC and SCC/SCC1 are intra-band, contiguous carriers, the same general rule was applied as in TRP in Table 6.2-2.

Example 14 (2 CA Intra-Band, Contiguous TIS): In this example, the PCC and SCC channels are chosen based on the same rule as TRP using Table 6.2-2..However, note that the high channel PCC and SCC are reversed from Table 6.2-2 because uplink operation is only allowed in the lower 70 MHz of Band 66 (exceptions for Band 66 are discussed in more detail in the next section).

CA_66C	66	66	20	20	66536	66734	100 RB with RBstart=0	100 RB with RBstart=0	100 RB with RBstart=0
			20	20	66786	66984	100 RB with RBstart=0	100 RB with RBstart=0	100 RB with RBstart=0
			20	20	67036	67234	100 RB with RBstart=0	100 RB with RBstart=0	100 RB with RBstart=0

Example 15 (3 CA with Intra-Band, Contiguous component TIS): In this example, the PCC and SCC1 follow the rule in Table 6.2-2 while SCC2 is chosen based on Table 6.2-3. However, note that the high channel PCC and SCC1 are reversed from Table 6.2-3 because uplink operation is only allowed in the lower 70 MHz of Band 66 (exceptions for Band 66 are discussed in more detail in the next section).

CA_66C-5A	66	SCC1=66 SCC2=5	20	SCC1=20 SCC2=10	66536	SCC1=66734 SCC2=2450	100 RB with RBstart=0	100 RB with RBstart=0	100 RB with RBstart=0	50 RB with RBstart=0
					66786	SCC1=66984 SCC2=2525	100 RB with RBstart=0	100 RB with RBstart=0	100 RB with RBstart=0	50 RB with RBstart=0
					67036	SCC1=67234 SCC2=2600	100 RB with RBstart=0	100 RB with RBstart=0	100 RB with RBstart=0	50 RB with RBstart=0

Example 16 (3 CA with Intra-Band, Contiguous component TIS): In this example, the intra-band, non-contiguous SCC1 and SCC2 follow the rule in Table 6.2-2 while the PCC is chosen based on Table 6.2-3.

CA_5A-66C	5	SCC1=66 SCC2=66	10	SCC1=20 SCC2=20	2450	SCC1=66536 SCC2=66734	25 RB with RBstart=25	50 RB with RBstart=0	100 RB with RBstart=0	100 RB with RBstart=0
					2525	SCC1=66786 SCC2=66984	25 RB with RBstart=25	50 RB with RBstart=0	100 RB with RBstart=0	100 RB with RBstart=0
					2600	SCC1=67036 SCC2=67234	25 RB with RBstart=25	50 RB with RBstart=0	100 RB with RBstart=0	100 RB with RBstart=0

Exceptions:

Some notable exceptions to the rules above include:

- TIS for 2A-2A and 5A-5A includes an extra test point due to desensitization when the SCC carrier frequency is below the PCC carrier frequency. These additional test points are based on the 3GPP TS 36.101 specifications for 2A-2A and 5A-5A.
- In some cases there are fewer than three test points depending on the size of the band and the channel bandwidth used for testing, e.g., 5B, 66D (TIS).
- Testing for 5A-5A uses 5 MHz channels instead of the normal 10 MHz based on expected deployment scenarios and the size of the band.
- Band 66 created deviations due to the nature of Band 66 having FDD operation in the lower 70 MHz of the band but downlink only operation in the upper 20 MHz of the band. These deviations are summarized below:
    - The PCC for the high channel is always at the upper edge of the 70 MHz FDD portion of the band.

- For TRP, Table 6.2-1 is replaced with Table 6.2-4 below for Band 66 intra-band, non-contiguous carriers (when the PCC is in Band 66):

Table 6.2-4 Band 66 Intra-Band, Non-Contiguous Carriers (When the PCC is in Band 66)

PCC	SCC or SCC1
Low Channel	High Channel
Mid FDD Channel	High Channel
High FDD Channel	Low Channel

Example 17 (2 CA Intra-Band, Non-Contiguous TRP for Band 66): In this example, the PCC and SCC channels are chosen based on the rules in Table 6.2-4.

CA_66A-66A	66	66	10	10	132022	67286	12 RB with RBstart=0	N/A	N/A
			10	10	132322	67286	12 RB with RBstart=19	N/A	N/A
			10	10	132622	66486	12 RB with RBstart=38	N/A	N/A

Example 18 (3 CA with Intra-Band, Non-Contiguous component TRP for Band 66): In this example, the PCC and SCC1 follow the rule in Table 6.2-4 while SCC2 is chosen to maximize the frequency span.

CA_66A-66A-5A	66	SCC1=66 SCC2=5	10	SCC1=10 SCC2=10	132022	SCC1=67286 SCC2=2450	12 RB with RBstart=0	N/A	N/A
					132322	SCC1=67286 SCC2=2450	12 RB with RBstart=19	N/A	N/A
					132622	SCC1=66486 SCC2=2450	12 RB with RBstart=38	N/A	N/A

For TIS, Table 6.2-1 is replaced with Table 6.2-5 below for Band 66 intra-band, non-contiguous carriers:

Table 6.2-5 Band 66 Intra-Band, Non-Contiguous Carriers

PCC	SCC or SCC1
Low Channel	High Channel
Low Channel	High FDD Channel*
Mid FDD Channel	Low Channel
High FDD Channel	Mid Channel

* NOTE: Only the “High FDD Channel” SCC is tested for this test point.

Example 19 (2 CA Intra-Band, Contiguous TIS for Band 66): In this example, the PCC and SCC channels are chosen based on the rule in Table 6.2-5. Note that for the test point in yellow, TIS testing is only required on the SCC.

CA_66A-66A	66	66	10	10	66486	67286	50 RB with RBstart=0	50 RB with RBstart=0	50 RB with RBstart=0
					66486	67086	50 RB with RBstart=0	50 RB with RBstart=0	50 RB with RBstart=0
					66786	66486	50 RB with RBstart=0	50 RB with RBstart=0	50 RB with RBstart=0
					67086	66786	50 RB with RBstart=0	50 RB with RBstart=0	50 RB with RBstart=0

Example 20 (3 CA with Intra-Band, Non-Contiguous component TIS for Band 66): In this example, the PCC and SCC1 follow the rule in Table 6.2-5 while SCC2 is chosen based on Table 6.2-3. Note that for the test point in yellow, TIS testing is only required on the SCC1 so the selection of SCC2 is arbitrary.

CA_66A-66A-5A	66	SCC1=66 SCC2=5	10	SCC1=10 SCC2=10	66486	SCC1=67286 SCC2=2450	50 RB with RBstart=0	50 RB with RBstart=0	50 RB with RBstart=0	50 RB with RBstart=0
					66486	SCC1=67086 SCC2=2525	50 RB with RBstart=0	50 RB with RBstart=0	50 RB with RBstart=0	50 RB with RBstart=0
					66786	SCC1=66486 SCC2=2525	50 RB with RBstart=0	50 RB with RBstart=0	50 RB with RBstart=0	50 RB with RBstart=0
					67086	SCC1=66786 SCC2=2600	50 RB with RBstart=0	50 RB with RBstart=0	50 RB with RBstart=0	50 RB with RBstart=0

Example 21 (3 CA with Intra-Band, Non-Contiguous component TIS for Band 66): In this example, the intra-band, non-contiguous SCC1 and SCC2 follow the rule in Table 6.2-5 while the PCC is chosen based on Table 6.2-3. Note that for the test point in yellow, TIS testing is only required on the SCC2 so the selection of the PCC is arbitrary. Note that for the test point in blue, the high channel for Band 66 was used (as opposed to the high FDD channel) since both Band 66 carriers are SCC's.

CA_5A-66A-66A	5	SCC1=66 SCC2=66	10	SCC1=10 SCC2=10	2450	SCC1=66486 SCC2=67286	25 RB with RBstart=25	50 RB with RBstart=0	50 RB with RBstart=0	50 RB with RBstart=0
					2525	SCC1=66486 SCC2=67086	25 RB with RBstart=25	50 RB with RBstart=0	50 RB with RBstart=0	50 RB with RBstart=0
					2525	SCC1=66786 SCC2=66486	25 RB with RBstart=25	50 RB with RBstart=0	50 RB with RBstart=0	50 RB with RBstart=0
					2600	SCC1=67286 SCC2=66786	25 RB with RBstart=25	50 RB with RBstart=0	50 RB with RBstart=0	50 RB with RBstart=0

Section 7 MU Analysis of Measurement Grids for mmWave Testing

The results tabulated in the tables below outline the results of a statistical analyses for the 8x2 antenna array while taking into account the positioning concept, i.e., the analyses were performed with the assumption that the beam peak direction is oriented away from the hemisphere towards the pole at $\theta = 180°$. Additionally, the standard deviations are presented when ranges of pattern values are disregarded (zeroed out). For the constant-step size measurement grids, three cases were investigated, i.e., no pattern values are disregarded, values only at one latitude at $\theta = 180°$, and the values at the bottom two latitudes are disregarded. For the constant density measurement grids, a similar investigation was performed using the Charged Particle implementation. Since there are no latitudes defined, the three cases investigated were: no pattern values are disregarded, values between $165° \leq \theta \leq 180°$, and values between $150° \leq \theta \leq 180°$are disregarded.

These results clearly show that for the measurement grids proposed in Section 6.1 and with the re-positioning concept considered, the measurements beyond 165º in θ can be skipped and interpolated instead. Alternate measurement grids listed in the tables below with larger number of grid points are not precluded where the measurements beyond 150º in θ can be skipped and interpolated instead provided that the standard deviation of 0.25 dB is met.

Table 7-1 Statistics of Quadrature Approaches for Constant Step Size Measurement Grids for the 8x2 Reference Antenna Array

Number Of		Number Of Latitudes Disregarded	Mean Error [dB]	STD. DEV [dB]	Min TRP Error [dB]	Max TRP Error [dB]	Quadrature	Re-Positioning Concept Applied
Latitudes	Longitudes							
13	24	0	0.00	0.06	-0.23	0.21	Clenshaw-Curtis	Yes
13	24	1	-0.01	0.07	-0.34	0.21	Clenshaw-Curtis	Yes
13	24	2	-0.08	0.15	-0.78	0.19	Clenshaw-Curtis	Yes
12	19	0	0.00	0.20	-0.97	0.76	Clenshaw-Curtis	Yes
12	19	1	-0.01	0.21	-0.94	0.77	Clenshaw-Curtis	Yes
12	19	2	-0.10	0.26	-0.96	0.77	Clenshaw-Curtis	Yes

Table 7-2 Statistics for Constant Density Measurement Grid Types for the 8x2 Reference Antenna Array (Charged Particle Implementation Only)

Number Of Grid Points	Range Of Angles Disregarded	Mean Error [dB]	STD. Dev [dB]	Min TRP Error [dB]	Max TRP Error [dB]	Re-Positioning Concept Applied
130	none	0.00	0.27	-0.95	0.81	yes
135	none	-0.01	0.22	-0.84	0.71	yes
140	none	0.00	0.19	-0.75	0.68	yes
145	none	-0.01	0.19	-0.61	0.58	yes
150	none	0.00	0.15	-0.60	0.53	yes
155	none	0.00	0.13	-0.42	0.52	yes
160	none	0.00	0.11	-0.41	0.43	yes
165	none	0.00	0.09	-0.40	0.39	yes
170	none	0.00	0.08	-0.36	0.37	yes
175	none	0.00	0.06	-0.27	0.29	yes
130	165°-180°	-0.05	0.29	-1.20	0.77	yes
135	165°-180°	-0.03	0.23	-1.18	0.67	yes
140	165°-180°	-0.05	0.22	-0.94	0.70	yes
145	165°-180°	-0.02	0.19	-0.82	0.57	yes
150	165°-180°	-0.03	0.16	-0.84	0.56	yes
155	165°-180°	-0.04	0.15	-0.74	0.48	yes
160	165°-180°	-0.04	0.13	-0.75	0.43	yes
165	165°-180°	-0.04	0.12	-0.71	0.36	yes
170	165°-180°	-0.04	0.12	-0.58	0.34	yes
175	165°-180°	-0.04	0.10	-0.65	0.27	yes
130	150°-180°	-0.16	0.35	-1.77	0.73	yes
135	150°-180°	-0.15	0.31	-1.93	0.63	yes
140	150°-180°	-0.18	0.30	-1.55	0.57	yes
145	150°-180°	-0.14	0.28	-1.29	0.54	yes

Number Of Grid Points	Range Of Angles Disregarded	Mean Error [dB]	STD. Dev [dB]	Min TRP Error [dB]	Max TRP Error [dB]	Re-Positioning Concept Applied
150	150°-180°	-0.15	0.25	-1.26	0.53	yes
155	150°-180°	-0.13	0.23	-1.09	0.46	yes
160	150°-180°	-0.16	0.24	-1.15	0.42	yes
165	150°-180°	-0.16	0.24	-1.12	0.32	yes
170	150°-180°	-0.15	0.23	-0.99	0.30	yes
175	150°-180°	-0.13	0.20	-0.90	0.28	yes

Appendix A Revision History

The change history only tracks changes that were directly applied to this document. Changes to earlier document versions that became necessary after a new major version was created are not tracked in this document's change history. For example, CTIA 01.01 v8.0.0 was based off of CTIA 01.01 v6.0.2 and subsequent revisions to CTIA 01.01 v6.0.2 are not included in the change history for CTIA 01.01 v8.0.x.

Date	Version	Description
February 2022	4.0.0	Initial release.
December 2022	5.0.0	Section 3 • Added Sections 3.9 through 3.12 for Average 3D C/N_0.
March 2023	6.0.0	Section 3 • Updated section 3.2, added Table 3.2-1 • Updated section 3.4 • Updated section 3.6 • Updated section 3.7
June 2024	6.0.1	Fixed unresolved cross references in document
April 2025	6.0.2	Section 3 • Corrected Upper Hemisphere 3D C/N_0 and Partial Isotropic GNSS 3D C/N_0 Equations 3.11-1 and 3.12-1 and added equations in Section 3.11 and 3.12 for 45 degree grids.